Article

Direct Gap Semiconductors Pb2BiS2I3, Sn2BiS2I3 and Sn2BiSI5

Saiful M. Islam, Christos D. Malliakas, Debajit Sarma, David C Maloney, Constantinos C. Stoumpos, Oleg Y. Kontsevoi, Arthur J. Freeman, and Mercouri G. Kanatzidis

Chem. Mater., **Just Accepted Manuscript** • DOI: 10.1021/acs.chemmater.6b02691 • Publication Date (Web): 15 Sep 2016

Direct Gap Semiconductors $Pb_2BiS_2I_3$, $Sn_2BiS_2I_3$ and Sn_2BiSI_5

Saiful M. Islam,[†] Christos D. Malliakas [†] Debajit Sarma,[†] David C. Maloney,[†] Constantinos C. Stoumpos, [†] Oleg Y. Kontsevoi, [§] Arthur J. Freeman, [§,] & Mercouri G. Kanatzidis[†,#]

†Department of Chemistry, [§]Department of Physics and Astronomy,
Northwestern University, Evanston, Illinois 60208, United States

We dedicate this work to the deceased Arthur J. Freeman

ABSTRACT: New quaternary thioiodides $Pb_2BiS_2I_3$, $Sn_2BiS_2I_3$, and Sn_2BiSI_5 have been synthesized by isothermal heating as well as chemical vapor transport. $Pb_2BiS_2I_3$ and $Sn_2BiS_2I_3$ crystallize in the space group, *Cmcm*, with unit cell parameters a = 4.3214 (9), b = 14.258 (3), and c = 16.488 (3) Å; a = 4.2890 (6), b = 14.121(2), and c = 16.414 (3) Å, respectively. Sn_2BiSI_5 adopts a unique crystal structure that crystallizes in *C*2/*m* with cell parameters a = 14.175 (3), b = 4.3985 (9), c = 21.625 (4) Å, and β = 98.90(3)°. The crystal structures of $Pb_2BiS_2I_3$ and $Sn_2BiS_2I_3$ are strongly anisotropic and can be described as three dimensional networks that are composed of parallel infinite ribbons of $[M_4S_2I_4]$ (M = Pb, Sn, Bi) running along the crystallographic c-axis. The crystal structure of Sn_2BiSI_5 is a homologue of the $M_2BiS_2I_3$ (M=Pb, Sn) which has two successive ribbons of $[M_4S_2I_4]$ separated by two interstitial ($Sn_{1-x}Bi_xI_6$) octahedral units. These compounds were characterized by scanning electron microscopy, differential thermal analysis, and X-ray photoelectron spectroscopy. $Pb_2SbS_2I_3$,

$Pb_2BiS_2I_3$, "$Pb_2Sb_{1-x}Bi_xS_2I_3$" (x~0.4), $Sn_2BiS_2I_3$ and Sn_2BiSI_5 are highly resistive that exhibit electrical resistivity of 3.0 GΩ·cm, 100 MΩ·cm, 65 MΩ·cm, 1.2 MΩ·cm and 34 MΩ·cm, respectively at room temperature. $Pb_2BiS_2I_3$, $Sn_2BiS_2I_3$, $Pb_2SbS_2I_3$, "$Pb_2Sb_{1-x}Bi_xS_2I_3$" (x~0.4), and Sn_2BiSI_5 are semiconductors with bandgaps of 1.60, 1.22, 1.92, 1.66 and 1.32 eV, respectively. The electronic band structures of $Pb_2BiS_2I_3$, $Sn_2BiS_2I_3$ and Sn_2BiSI_5, calculated using density functional theory, show that all compounds are direct bandgap semiconductors.

Deceased: Arthur J. Freeman
Department of Physics and Astronomy,
Northwestern University, Evanston, Illinois 60208, United States

INTRODUCTION

Hetero-anionic inorganic compounds define a unique class of materials which contain at least two different anionic species in their structures, and they can exhibit exceptional physical and chemical properties.[1-7] Their chemistry is not as well developed as that of homo-anionic compounds. Because of the variance in electronegativity, ionic charge, charge densities, polarizability, and other physico-chemical properties different anions exhibit diverse bonding propensities towards metal cations. When occurring in the same lattice these differences result in different coordination preferences and diverse structural fragments to generate novel composite crystal structures with unique properties. For example, the hetero-anionic compounds Tl_6SeI_4[5] and SbSeI[8] show promise in nuclear radiation detection, BiOI can be used as photo-catalyst for water purification,[9-10] $AgNa(VO_2F_2)_2$ is used as cathode material for electrochemical energy storage,[11] oxypicnides *Ln*FeO*Pn* (Pn = P, As, *Ln* = rare-earth)[3, 12-16] evolved as high T_c superconductors, BiOCuSe exhibits enhanced thermoelectric properties, LaCuO*Q* and BaCu*Q*F (Q = S, Se, Te)[17-20] act as transparent conducing semiconductors, and $Ba_3AGa_5Se_{10}Cl_2$(A=Cs, Rb, K),[2] $(Sb_7S_8Br_2)(AlCl_4)_3$,[21] $(Hg_6P_3)(In_2Cl_9)$[6] and $(Hg_8As_4)(Bi_3Cl_{13})$[6] are interesting due to their strong second harmonic generation (SHG) properties.[22]

One of the subclasses of hetero-anionic inorganic compounds is chalco-halides. This class of compounds exhibits unusual structures which are the results of the distinct bonding preferences of chalcogenide and halide atoms as they compete for a stable site in the structure. Notable examples include $CuCr_2Se_{4-x}Br_x$,[1] $MnSbS_2Cl$,[23] $MnSbSe_2I$,[24] Ni_8Bi_8SI,[25] $CdSb_6S_8I_4$,[26] $LnSbS_2Br_2$ (Ln = La, Ce),[27] $LaSbS_5Br$,[28] $LaCa_2GeS_4Cl_3$,[29] $Cu_3Bi_2S_4Br$,[30] and $AE_2Sb_2Q_4F_2$ (AE = Sr, Ba; Q = chalcogen),[31] $InBi_2S_4Cl$,[32] $Cu_2Cu_{2-x}(Pb_{1-x}Bi_x)Bi_2S_5I_2$,[33] $CdSb_6S_8I_4$,[26] $SnSb_2SI_6$,[34] $Sn_2SbSe_2I_3$,[34]

$Sn_3SbSe_2I_5$,[34] Hg_3AsSe_4I,[35] $Sn_2SbS_2I_3$,[36-37] $Pb_2SbS_2I_3$,[37-38] Bi_2CuSe_3I,[39] $Bi_6Cu_3S_{10}I$[39] and the mineral mutnovskite Pb_2AsS_3(I, Cl, Br).[40]

In this contribution, we report the syntheses and crystal structures of three novel sulfo-iodides, $Pb_2BiS_2I_3$, $Sn_2BiS_2I_3$, and Sn_2BiSI_5. The materials are direct bandgap n-type semiconductors with bandgaps ranging between 1.2-1.6 eV and exhibit high electrical resistivity (> 1 MΩ·cm).

EXPERIMENTAL SECTION

Synthesis

BiI_3 and SbI_3: Antimony and bismuth iodides were synthesized by the melt-quench technique in a fast heating furnace. For SbI_3, a mixture of antimony (363.0 mg; 3 mmol, 99.999% Alfa Aeser), and iodine (1146 mg; 9.01 mmol; 99 +% Sigma Aldrich) were combined in an evacuated sealed silica tube (l = 11 cm, 9 mm inner diameter). The reactants were melted in the furnace at 400°C and subsequently quenched in water. Initially during heating the interior of the tubes had a dark color due to liberation of iodine gas. Subsequent melting-quenching cycles (7-8 cycles in ~ ½ h) allowed for the complete reaction of iodine evidenced by the disappearance of the dark gas inside the tubes. Finally, the tubes were heated at 450°C for about an hour and quenched in air to form SbI_3 (red). To synthesize BiI_3 (black), (bismuth (629.7 mg; 3 mmol; 99.999% Alfa Aeser), and iodine (9.01 mmol, 99+% Sigma Aldrich) were loaded in an evacuated sealed silica tube (l = 11 cm, 9 mm inner diameter) and the same heat treatment was used as described for SbI_3 (red).

SnS: 7.8736 g of tin (American Elements, 99.999%) and 2.1264 g sulfur (Sigma Aldrich, 99.99%) were combined in a fused silica tube (l = 30 cm, 8 mm inner diameter, ID). The first tube was then sealed under a pressure of 5×10^{-4} Torr and sealed inside a second tube (15 mm ID) under a pressure of 9×10^{-3} Torr. The system was then heated to 400°C in 4 hours, 450°C in 5

hours, 1000°C in 11 hours, and held at that temperature for 5 hours. The tube was finally allowed to cool to 610°C in 20.5 hours, 590°C in 20 hours, and then to room temperature in 11 hours. **Caution**: It is important to follow this procedure closely to prevent the tubes from bursting catastrophically. This is because sulfur has a high vapor pressure and if it fails to react with Sn metal due to passivation of the surface it can burst the inner tube. The heating profile, tube sizes, pressures, and reactant mass were chosen to minimize the effect of sulfur's high vapor pressure and to ensure that as much sulfur as possible had reacted before reaching its boiling point. Furthermore, SnS has a phase transition at 600°C where it expands on cooling breaking the inner tube. The cooling temperature program was chosen so that the inner tube breaks gently and does not shatter the outer tube. If the outer tube breaks on heating or cooling while the reactants are at high temperature the reactants will oxide violently.

PbS. Was synthesized by heating a stoichiometric mixture of elemental lead (8288 mg, 40mmol) (99.999% Alfa Aeser) and sulfur (1280 mg, 40mmol) (99.98% 5N Plus Inc.) to 400°C in 24h and holding for 24h and then the temperature was raised to 900°C in 24h followed by a subsequent soaking for 48h and finally cooled down to room temperature in 12 h.

$Pb_2BiS_2I_3$. $Pb_2BiS_2I_3$ was obtained with a yield of ~ 90% (weight) by heating a stoichiometric mixture of PbS (2.871mg, 12 mol) and BiI_3 (3.538g, 6 mol) at 500°C for 48h, holding for 72h, and cooling down to room temperature in 24h all in a sealed silica tube (l = 12 cm, width 9 mm inner). This procedure led to black well-formed needle-like crystals $Pb_2BiS_2I_3$ up to ~ 2 mm in length (Figure 1). Attempting to synthesis from a stoichiometric mixture of elemental Pb (414.4 mg, 2 mmol), Bi (209.0 mg, 1.0 mmol), sulfur (64.0 mg, 2 mml) and iodine (~380 mg, 3 mmol) resulted in a mixture of $Pb_2BiS_2I_3$, BiSI[41] and PbI_2.

$Sn_2BiS_2I_3$ and Sn_2BiSI_5: $Sn_2BiS_2I_3$ was synthesized from a melted mixture of elemental tin (238.7 mg, 2 mmol; 99.999% Alfa Aeser), bismuth (209.0 mg, 1 mmol; 99.999% Alfa Aeser), sulfur (64.0 mg, 2 mmol; 99.98% 5N Plus Inc.) and iodine (400 mg, 3.15 mmol; 99+%, Sigma Aldrich). The reactants were heated in evacuated sealed silica tube (l = 12 cm, inner width 9 mm) for 72h to 500^{o}C, held at that temperature for 24h, and finally cooled to room temperature in 96 h. This procedure led to the formation of mainly $Sn_2BiS_2I_3$ (black, Figure 1) along with Sn_2BiSI_5 (black, Figure 1), SnS_2 (yellow), and BiSI (needles). The sulfo-iodide, $Sn_2BiS_2I_3$ was also synthesized from a melted mixture of SnS (150.8 mg; 1 mmol), BiI_3 (294.8 mg; 0.5 mmol) in sealed silica tube (yield ~90% by weight). The reactants were melted and water quenched repeatedly in a melting furnace at 420 and 520^{o}C (seven to eight melting-quenching cycles). The tube was then kept in the furnace at 520^{o}C for about 3 h and then the furnace was shut down for cooldown to room temperature. This melting quenching cycles are required to capture the dissociated iodine from BiI_3 to react with SnS and to form $Sn_2BiS_2I_3$.

In order to synthesize Sn_2BiSI_5, a stoichiometric mixture of Sn (119.9 mg, 1 mmol), Bi (106.1 mg, 0.5 mmol), S (18.2 mg, 0.5mmol) and I (320.0 mg, ~2.5 mmol) was loaded in a silica glass tube, vacuum sealed and melted at 400^{o}C and then water quenched. This melting and quenching processes continued several times until most of the iodine had reacted. This was determined by observing the gradual disappearance of purple vapor in the tubes till they were almost colorless. Afterwards, the tube was transferred into a furnace and heated to 500°C in 24h then held for 24 h and cooled down to room temperature in 48 h. This procedure led to the formation of Sn_2BiSI_5, $Sn_2BiS_2I_3$, and an unknown impurity (identified X-ray powder diffraction) at the bottom of the tube (reactant containing high temperature end) with a yield of about 70% while a small amount of Sn_2BiSI_5 and "unknown impurity" (∑~50 mg) were transported to other side of the tube

(cooler end) due to small temperature gradient ($\Delta T \sim 25^{o}C$) in the furnace. Sn_2BiSI_5 can be easily separated from "unknown impurity" by washing the solid mixture with ethanol where the latter is soluble.

"$Pb_2Sb_{1-x}Bi_xS_2I_3$": "$Pb_2Sb_{1-x}Bi_xS_2I_3$" (x~0.4) was synthesized aiming for a stoichiometric composition of $Pb_2Sb_{0.5}Bi_{0.5}S_2I_3$. A mixture of PbS (478.6 mg; 2 mmol), Bi (105.0 mg; ½ mmol) Sb (61.0 mg, ½ mmol), sulfur (64.0 mg, 2 mml) and iodine (~380 mg, 3 mmol) was heated to $500^{o}C$ in 48h, holding for 72h, and cooling down to room temperature in 24h in an evacuated sealed silica tube (l = 12 cm, inner width 9 mm). This procedure led mainly to "$Pb_2Sb_{1-x}Bi_xS_2I_3$" (x~0.4), along with other minor phases BiSI,[41] SbSeI,[8] and PbI_2 which were identified by X-ray powder diffraction as well EDS (Energy Dispersive X-ray Spectroscopy) analyses.

Powder X-ray Diffraction. Powder X-ray diffraction (PXRD) data were collected on ground crystalline samples of $Pb_2BiS_2I_3$, $Sn_2BiS_2I_3$, and Sn_2BiSI_5 with a flat sample geometry using a silicon-calibrated CPS 120 INEL powder X-ray diffractometer (Cu Kα graphite-monochromatized radiation) operating at 40 kV and 20 mA equipped with a position-sensitive detector. Simulated patterns were generated using the CIF of each refined structure and the Visualizer program within FindIt.[42]

Scanning Electron Microscopy. Images and semi-quantitative energy dispersive X-ray spectroscopy (EDS) analyses of $Pb_2BiS_2I_3$, $Sn_2BiS_2I_3$, "$Pb_2Sb_{1-x}Bi_xS_2I_3$" (x~0.4) and Sn_2BiSI_5 were obtained using a Hitachi S-3400 scanning electron microscope equipped with a PGT energy-dispersive X-ray analyzer. For the analysis single-crystals of the above thioiodides were selected under the optical microscope and placed on the surface of the double sided carbon tape which was already attached on the flat surface of the SEM stubs. For EDS analysis spectra were collected using an accelerating voltage of 15 kV and a 90 s accumulation time. These analyses

show the homogeneous distribution of the respective atoms with the atomic ratio close to their corresponding chemical compositions (Figure S1-S4). The compositions obtained as Pb=26.94%, Bi=12.06%, S=23.92%, and I=37.08% % for $Pb_2BiS_2I_3$ (Figure S1); Pb=26.75%, Sb= 6.89%, Bi=5.92%, S=23.63%, and I=36.81% for"$Pb_2Sb_{1-x}Bi_xS_2I_3$" (Figure S2); Sn=23.47%, Bi=14.54%, S=27.5%, and I=34.49% for $Sn_2BiS_2I_3$ (Figure S3); and Sn=25.97%, Bi=13.22%, S=11.23%, I=49.58% (Figure S4) for Sn_2BiSI_5.

Single-Crystal X-ray Crystallography. X–ray single crystal data collection of $Pb_2BiS_2I_3$, $Sn_2BiS_2I_3$, and Sn_2BiSI_5 were performed on a STOE IPDS II or a STOE IPDS 2T diffractometer using Mo Kα radiation (λ = 0.71073 Å) and operating at 50 kV and 40 mA at 293 K. Integration and numerical absorption corrections were performed using X-AREA, X-RED, and X-SHAPE. All structures were solved using direct methods and refined by full-matrix least squares on F^2 using the SHELXTL program package. The crystal structure refinement of $Sn_2BiS_2I_3$ exhibits two distinct crystallographic sites 8*f* and 4*c* for metal atoms where the 8*f* Wyckoff site is mixed occupied ($Sn_{1-x}Bi_x$) and the 4*c* site is exclusively occupied by Sn atom. In contrast to the straightforward refinement of the crystal structure of $Sn_2BiS_2I_3$ the refinement of the crystal structure of $Pb_2BiS_2I_3$ was indistinct due to the very similar X-ray scattering power of lead (*Z*=82) and bismuth (*Z*=83). $Pb_2BiS_2I_3$ is isostructural to $Sn_2BiS_2I_3$ and thus the 4*c* site is occupied by the divalent Pb atom and 8*f* site is shared by Pb and Bi atoms. Because of similar atomic number Z of Pb and Bi, the occupancy of the mixed 8*f* site was fixed to 50% of each element in the final step of the refinement. This gives a composition $Pb_2BiS_2I_3$ which is consistent with the EDS analysis. According to bond valence sum calculations[43] on $Pb_2BiS_2I_3$ the unique Pb site exhibits BVS ~ 2.04 v.u. and for the mixed ($Pb_{0.5}Bi_{0.5}$) sites BVS is 2.54 v.u. These values are in good agreement with the respective charge of Pb^{2+} and mixed

$(Pb_{0.5}^{+2}Bi_{0.5}^{+3})^{+2.5}$. A complete list of crystallographic information, data collections, structure refinements, atomic coordinates, thermal displacement parameters, and selected inter atomic distances and angles are given in Table 1 and 3.

X-ray Photoelectron Spectroscopy (XPS). X-ray photoelectron studies were performed using a Thermo Scientific ESCALAB 250 Xi spectrometer equipped with a monochromatic Al Kα X-ray source (1486.6 eV) and operated at 300 W. Samples were analyzed under vacuum ($P < 10^{-8}$ mbar), whereas survey scans and high-resolution scans were collected using pass energy of 50 eV. Binding energies were referred to the C 1s binding energy at 284.6 eV. A low-energy electron flood gun was employed for charge neutralization and ion beam etching for surface cleaning. Prior to XPS measurements, ground crystals of each sample attached on copper foil and mounted on stubs and successively put into the entry-load chamber to pump.

Resistivity and Seebeck Measurements. Resistivity measurements were conducted using a homemade apparatus equipped with a nanovoltmeter (Keithley 2182A), an electrometer (Keithley 6517), and a high-temperature vacuum chamber governed by a temperature controller (MMR Technologies K-20). For the Seebeck coefficient measurement, needle-like crystals were mounted on the stage and attached to the thermocouples with colloidal graphite liquid. The Seebeck voltage $V(T)$ was measured by the integral method, in which one end of the sample is held at a fixed temperature T_0, and the other end is varied through the temperature T range of interest using a commercial MMR Technologies SB-100 Seebeck measurement system. The Seebeck coefficient S is obtained from the slope of the $V(T)$ vs T curve, i.e., $S = dV(T)/dT$.[44]

Band Structure Calculations. In order to investigate the electronic structure of $Pb_2BiS_2I_3$, $Sn_2BiS_2I_3$ and Sn_2BiSI_5, first-principles calculations were carried out within the density functional theory formalism using the Projector Augmented Wave method[45] implemented in

Vienna Ab-initio Simulation Package[46-47]. The energy cut off for planewave basis was set to 350 eV. The generalized gradient approximation (GGA), functional of Perdew−Burke−Ernzerhof (PBE)[48], was employed. The crystal structures and the lattice parameters were fixed to their experimentally observed values, but the positions of atoms in the cells were relaxed until the atomic forces on each atom are less than 0.01 eV/Å. The Monkhorst-Pack k-point grids of 12×12×3, 12×4×3, and 12×12×2 were used for Brillouin zone (BZ) sampling for $Pb_2BiS_2I_3$, $Sn_2BiS_2I_3$, and Sn_2BiSI_5, respectively.

RESULTS AND DISCUSSION

Syntheses, purification and thermal behavior. $Pb_2BiS_2I_3$ and $Sn_2BiS_2I_3$ were synthesized by slowly cooling a melted mixture of PbS with BiI_3, and SnS with BiI_3, in a molar ratio of 2:1 in sealed silica tubes at 500°C. The synthesis of $Pb_2BiS_2I_3$ and $Sn_2BiS_2I_3$ from their direct elemental combination led to the formation of mixtures of the binary compounds PbI_2, SnI_4, and SnS_2, or ternary compounds such as BiSI, alongside the dominant desired products. The formation of the binary and ternary impurities along with the desired product could be due to the loss of iodine gas from the reaction mixture that eventually results in a change in the stoichiometry of the reaction. Attempts to synthesize a single phase product of Sn_2BiSI_5 resulted in the formation of black needles of $Sn_2BiS_2I_3$, Sn_2BiSI_5, and unknown impurities at the bottom (high temperature end) of the silica tube while Sn_2BiSI_5 is transported in the other end (low temperature end).

$Pb_2BiS_2I_3$, $Sn_2BiS_2I_3$, Sn_2BiSI_5 and "$Pb_2Sb_{1-x}Bi_xS_2I_3$" (x~0.4) are stable in air and insoluble in water, acetone, ethanol, formamide, DMF, and hydrazine. Differential thermal analysis (DTA) was performed on ground crystals of $Pb_2BiS_2I_3$ (Figure 2A) which showed that the compound melts incongruently at 455°C and crystallizes at 410°C. Careful inspection of the DTA tube

revealed the existence of yellow PbI_2. This provides evidence of the incongruent melting behavior of $Pb_2BiS_2I_3$. Thermogravimetric analysis (TGA) under nitrogen atmosphere also showed that $Pb_2BiS_2I_3$ starts to decompose at about 460^{o}C (Figure 2B) and thus in agreement with its incongruent melting behavior. Due to the high volatility of iodine we anticipate other thiohalides behave similarly to the $Pb_2BiS_2I_3$.

Crystal structures. $Pb_2BiS_2I_3$ and $Sn_2BiS_2I_3$ crystallize in centrosymmetric space group, *Cmcm*, and are isostructural to $Pb_2SbS_2I_3$.[37, 49] The crystal structure refinement was forthright for $Sn_2BiS_2I_3$, however, because of very similar atomic scattering power of lead and bismuth assignment of their positions in the crystal structure of $Pb_2BiS_2I_3$ was supported by chemical analyses of its isostructural thiohalides, bond valence sum calculation[43], EDS analyses (discussed in detail in experiment section, Figure S1) as well as the minimal energy at different distribution of metals at different crystallographic sites during electronic band structure calculations. $Pb_2BiS_2I_3$ and $Sn_2BiS_2I_3$ exhibit a statistically disordered structure where one M^{2+} (M=Pb or Sn) cations exclusively occupy 4*c* crystallographic site while a mixed occupancy exists $(M_{0.5}{}^{2+}Bi_{0.5}{}^{3+})^{+2.5}$ at the 8*f* Wyckoff site (Figure 3). This distribution of cations was also observed in the crystal structure of $Sn_2SbS_2I_3$ where Sn and Sb also have very similar atomic number.[37]

The crystal structure of $Pb_2BiS_2I_3$ can be simply described as parallel infinite chains of $[(Pb_{0.5}Bi_{0.5})_2S_2]$ extending along the crystallographic *a*-axis (Figure 3B). These chains are interconnected by trigonal prismatic $[PbI_6]$ polyhedra through face-sharing to give a rigid two-dimensional network along *c*-axis. A weak $(Pb_{0.5}Bi_{0.5})$-I ~ 3.80 Å interaction (as compared to d(Pb-I)=3.21 Å in PbI_2) extend the crystal structure along the crystallographic *b*-axis and thus provides a three-dimensional feature of the crystal structure.

Similar structural topographies are observed for $Sn_2BiS_2I_3$ where an infinite chain of $[(Sn_{1-x}Bi_x)_2S_2]$ (x~0.5) running along the crystallographic *a*-axis and are interconnected by trigonal prismatic $[SnI_6]$ polyhedra (Figure 3D). An alternative description of the crystal structures of $Pb_2BiS_2I_3$ and $Sn_2BiS_2I_3$ are as the assembly of infinite $[((Pb_{0.5}Bi_{0.5})_2Pb_2S_2I_4]$ or $[(Sn_{1-x}Bi_x)_2Sn_2S_2I_4]$ (x~0.5) ribbons ($[M_4S_2I_4]$; *M* = Pb, Sn, Bi), respectively running along the crystallographic *c*-axis (Figure 3A-B with gray shaded regions). Interestingly, these ribbons are arranged in such a way that essentially form a two dimensional crystal structure (Figures 3B and 3D) along *ac* plane of the crystal structure. A weak interaction between *M* and I, *d*(*M*-I) = ~ 3.80 Å (*M* = PbBi, SnBi) provides the 3D-like character of the crystal structures $Pb_2BiS_2I_3$ and $Sn_2BiS_2I_3$.

Like $Sn_2BiS_2I_3$, Sn_2BiSI_5 exhibits a statistical disorder in its crystal structure (Figure 4A, B). In case of Sn_2BiSI_5, the $[(Sn_{1-x}Bi_x)_2S_2]$ (x~0.5) chains are extended along the crystallographic *b*-axis and two successive chains are inter connected by a trigonal prismatic $[SnI_6]$ and two $(Sn_{1-x}Bi_xI_6)$ octahedral unit (Figure 4E, F) along the *c*-axis. The second approach is to describe the structure as an infinite ribbon $[M_4S_2I_4]$ (*M* = Sn, Bi) running along the crystallographic *c*-axis. Two adjacent ribbons parallel to the *a*-axis are separated by two $(Sn_{1-x}Bi_xI_6)$ (x~0.5) octahedral unit which reveals a void of ~18Å in length along the *c*-axis. The accommodation of such $(Sn_{1-x}Bi_xI_6)$ octahedra into the structure of $Sn_2BiS_2I_3$ results in the increase of the crystallographic *c*-axis from ~16.4 to 21.6 Å for Sn_2BiSI_5. Like $Sn_2BiS_2I_3$, a weak bonding interaction between $(Sn_{1-x}Bi_x)$ and iodine (*M*-I=~3.8Å) is again indicative of the 3D character of the crystal structure of Sn_2BiSI_5. It is noteworthy to mention that a very similar ribbon of $[M_4S_2I_4]$ (*M*=Pb) also exists in the crystal structure of the $Pb_5S_2I_6$ (Figure 4C).[50] In $Pb_5S_2I_6$ two adjacent ribbons $[Pb_4S_2I_4]$ are interconnected along the *c*-axis by two isolated $[PbI_6]$ octahedra that leave a void of ~7.5Å. Each

of the two [PbI_6] octahedra in $Pb_5S_2I_6$ also connects [$Pb_4S_2I_4$] ribbons along the [211] lattice plane, however, this kind of building feature is completely missing in the crystal structure of Sn_2BiSI_5. Finally, we conclude that despite the difference in connectivity of [$M_4S_2I_4$], all thiohalides of $M_2BiS_2I_3$ (M = Sn, Pb), Sn_2BiSI_5, and $Pb_5S_2I_6$ are structurally closely related. A homologous series can be defined where the crystal structure of $M_2BiS_2I_3$ consists of an infinite ribbon [$M_4S_2I_4$]m=α (M = Sn, Pb, Bi) while for $Pb_5S_2I_6$ and Sn_2BiSI_5, the ribbon is separated by one [MI$_6$] and two [MI$_6$] octahedra, respectively. If a homologous series does exist in this family then several more members with predictable structure and compositions could be expected to form.[51-52]

The coordination environments, interatomic distances and angles $Pb_2BiS_2I_3$, $Sn_2BiS_2I_3$, and $Sn_2BiS_2I_5$ are given in Figure 5 and Tables 4-6. Because of the isostructural character of $Pb_2BiS_2I_3$ and $Sn_2BiS_2I_3$, the metals atoms exhibit similar coordination environments. In $Pb_2BiS_2I_3$, ($Pb_{0.5}Bi_{0.5}$) forms 8-fold coordination polyhedra as [$Pb_{0.5}Bi_{0.5}S_3I_5$] where the d(Pb1-S1) shows one short bond 2.638 Å and two long bonds 2.737Å. The d[($Pb1_{0.5}Bi1_{0.5}$) -I)] distances can be classified as long (d[($Pb_{0.5}Bi_{0.5}$) -I1)] = 3.770 Å), intermediate d[($Pb_{0.5}Bi_{0.5}$)-I2)] = 3.670Å), and short (d[($Pb_{0.5}Bi_{0.5}$)-I2)] = 3.454Å). When all bonding interactions are considered the polyhedron adopts a distorted bicapped-trigonal prismatic coordination environment. The unique Pb atom (at 4c site) also adopts a bicapped trigonal prismatic coordination with six iodine atoms assembling the trigonal prism, two additional sulfur atoms capping the square faces of the prism thus completing the 8-fold coordination of the [PbI_6S_2] polyhedra. In this polyhedron, d(Pb2-I) inter atomic distances can be classified as short and long d(Pb2-I) = 3.134 and 3.600Å, respectively. In $Sn_2BiS_2I_3$, the coordination polyhedra of ($Sn2_{1-x}Bi1_x$) (x~0.5) appear as [($Sn2_{1-x}Bi1_x$)S_3I_5] (3×d((Sn2Bi)-S1) = 2.562-2.726Å and 5×d((Sn2Bi1-I) ranging from 3.353 to

3.817Å) and coordination environment of Sn1 comprises of two sulfur (2×*d*(Sn1-S1) = 2.921Å) and six iodine atoms (2×*d*(Sn1-I2) = 3.029 Å and 4×*d*(Sn1-I1) = 3.649 Å)) atoms.

The crystal structure of Sn_2BiSI_5 consists of [(Bi2ASn2A)S_3I_5] (Bi2A~Sn2A~0.5), [Sn3SI_6] and [(Bi1ASn1A)I_6] (Bi1A~Sn1A~0.5). The coordination polyhedra of [(Bi2ASn2A)S_3I_5] (3×*d*((Bi2ASn2A)-S1) ~ 2.637 to 2.722Å) and 5×*d*(Bi2ASn2A-I) ~ 3.472 to 3.802 Å) and [Sn3SI_6] (*d*(Sn3-S1) = 2.677Å and *d*(Sn3-I) distances ranging from 3.079 to 3.715Å and the Sn3-I1 distance is 4.152Å and the latter remains just at the boundary of the sum of their van der Waals radii that represents very weak interactions.

X-ray Photoelectron spectroscopy. $Pb_2BiS_2I_3$, $Sn_2BiS_2I_3$ and Sn_2BiSI_5 were characterized by X-ray photoelectron spectroscopy (Figure 6). Table 7 shows the binding energies of the representative orbitals of each element in these thioiodides. The splitting of the binding energy of 4*f* orbitals in lead and bismuth, and the energies of the 3*d* orbitals for tin and iodine are attributed to the strong spin-orbit coupling. The binding energy of lead 4*f* is assigned as 143.34 ($4f_{5/2}$) and 138.43 ($4f_{7/2}$) eV which is consistent with +2 oxidation states of lead in $Pb_2BiS_2I_3$ and thus in agreement with its crystal structure.[53] In all the three thioiodides the binding energies of Bi 4*f* are very similar (~159 ($4f_{7/2}$), ~164 ($4f_{5/2}$) eV) and are corresponding to their +3 oxidation states.[53] In addition, the very similar binding energies of bismuth in these thioiodides are indicative for their very similar chemical environments. The binding energies at 486.73 (495.12) and 487.23 (495.76) eV are attributed to Sn $3d_{5/2\,(3/2)}$ energies of $Sn_2BiS_2I_3$ and Sn_2BiSI_5, respectively.[54]

Optical and electronic properties. $Pb_2BiS_2I_3$, $Sn_2BiS_2I_3$, "$Pb_2Sb_{1-x}Bi_xS_2I_3$" (x~0.4), and Sn_2BiSI_5 are black in color which is in agreement with their experimental optical band gaps 1.60, 1.22, 1.66 and 1.32 eV, respectively (Figure 7). The antimony analogue $Pb_2SbS_2I_3$ exhibits a bandgap of ~1.92 eV which is close to the value (E_g~2.0 eV) reported by Starosta *et al*.[38] The

bandgap of $Pb_2BiS_2I_3$ is about ~0.32 eV lower than that of $Pb_2SbS_2I_3$. This can be understood by the greater degree of extension of the atomic orbitals and higher spin orbit coupling of the bismuth atom. Interestingly, despite the smaller cationic size of tin the bandgap of $Sn_2BiS_2I_3$ is about 0.4 eV lower than that of its lead analogue $Pb_2BiS_2I_3$. Similar findings are observed for $Sn_2SbS_2I_3$ and $Pb_2SbS_2I_3$. The high energy of the delocalized lone $5s^2$ pair of electrons on the Sn^{2+} cation could explain such lowering of bandgaps.[55-56] In all cases we observe sharp absorption edges in the spectra which are suggestive of a direct electronic transition from the valence band to conduction band, a statement which is supported by the electronic structure calculations (vide infra).

The room temperature electrical resistivity of $Pb_2SbS_2I_3$, $Pb_2BiS_2I_3$, "$Pb_2Sb_{1-x}Bi_xS_2I_3$" (x~0.4), $Sn_2BiS_2I_3$, and Sn_2BiSI_5 measured by a two-point contact along the crystallographic *c*-axis which is the long-axis of the needle-shaped crystals. This thioiodides are highly resistive and exhibit electrical resistivity as 3.0 GΩ·cm, 100 MΩ·cm, 65 MΩ·cm, 1.2 MΩ·cm, and 34 MΩ·cm, respectively (Figure 8). These values of the resistivity of the isostructural compounds $A_2BS_2I_3$ (*A* = Sn, Pb, and *B* = Sb, Bi) are in agreement with the trend in their optical bandgaps, with the highest resistivity sample exhibiting the highest optical bandgap. The Seebeck coefficients for all samples were negative and very large, between ~ -1500 uV/K for $Pb_2BiS_2I_3$ and ~ -3000 uV/K for $Sn_2BiS_2I_3$, indicating an intrinsic semiconducting behavior (Figure S5) with a very low number of charge carriers. The thermal conductivity of $Pb_2BiS_2I_3$ was measured from 100 to 400°C and the values were found to be very low ranging from 0.7 to 1.2 W/m K (See supporting information, Figure S6).

Band structure calculations

In order to better understand the nature of the semiconducting character and electronic transitions in $Pb_2BiS_2I_3$, $Sn_2BiS_2I_3$, and Sn_2BiSI_5 we performed electronic band structure calculations (Figure 9-11). With the PBE exchange-correlation functional the bandgaps are predicted to have values of 1.18, 0.90, and 0.85 eV for $Pb_2BiS_2I_3$, $Sn_2BiS_2I_3$, and Sn_2BiSI_5, respectively, which are underestimated compared to the experimental values of 1.60, 1.22, and 1.32 eV. This underestimation of bandgaps compared to the experimentally obtained values is a well-known tendency of semi-local functionals like GGA.[57-58]

$Pb_2BiS_2I_3$ has mixed occupancy of Pb and Bi at the 8*f* crystallographic site. In order to perform the electronic structure calculations, a structural model was created that approximates mixed occupation of these sites by a periodic array of sites occupied by either Pb or Bi. An unlimited number of such models can be proposed with different arrangements and short- and long-range order within the Pb/Bi sublattice. A model utilized in this work employs a conventional unit cell which has double the number of atoms compared with the primitive unit cell, and has the orthorhombic primitive lattice instead of orthorhombic *C*-centered lattice of the primitive unit cell. Such cell is the smallest possible unit cell and therefore has the highest degree of order.

The calculated electronic structure of $Pb_2BiS_2I_3$ is shown in Figure 9 in the form of (a) the electronic band structure plotted along the lines between the high-symmetry points in the BZ and (b) the electronic density of states (DOS) projected onto the atomic sites. The valence band (VB) maximum (VBM) and the conduction band (CB) minimum (CBM) are both located at the Γ point revealing that $Pb_2BiS_2I_3$ is a direct bandgap material. This result is in agreement with the sharp nature of the absorption edges observed from its experimental spectrum. It should be noted that the VB is very flat near the VBM and it extends toward the Y point, while, in contrast, the CB near the CBM shows a significant dispersion. This will result in a large hole effective mass

but a small electron effective mass. From the DOS picture it can be seen that the VBM is formed almost exclusively by hybridized S *p* and I *p* states, and there is little contribution from Pb and Bi. In contrast, the CBM is dominated by Bi *p* hybridized with I *p* and, to the lesser degree, S *p* states.

Similarly to $Pb_2BiS_2I_3$, $Sn_2BiS_2I_3$ has mixed occupancy of Sn and Bi on the 8*f* site, so the same structural model was employed in the calculations. The calculated electronic structure is presented in Figure 10 in the form of the electronic band structure and the DOS shows a number of features that are very similar to the electronic structure of $Pb_2BiS_2I_3$. $Sn_2BiS_2I_3$ is also a direct-gap material, with the band gap at the Γ point. The VB near VBM is extremely flat extending almost all the way towards both Y and Z points, while CBM exhibits a significant dispersion. The composition of VMB is more complex than in $Pb_2BiS_2I_3$: the VBM is similarly consists of hybridized S *p* and I *p* states, but in addition there is a significant contribution from Sn2 5*s* states. This results from the fact that Sn 5*s* states have higher energy than the corresponding Pb states. By hybridizing with S *p* and I *p* states near the VBM, Sn *s* states effectively push VBM up, which in effect leads to the band gap suppression in $Sn_2BiS_2I_3$ compared to $Pb_2BiS_2I_3$. Interestingly, there is no contribution to the VBM from Bi states, even though Bi atoms occupy the same mixed positions as Sn2 atoms. Instead, Bi *p* states contribute to the CBM, where they hybridize with I *p* states together with Sn1 *p*. This result emphasizes that interaction of Sn and Bi atoms with their neighbors plays a critical role in formation of VBM and CBM, respectively.

Sn_2BiSI_5 is also a disordered phase, in which an intermixture of Bi and Sn exists on sites 1 and 2 (see Table 2). For the electronic structure calculations, a simplified crystal structure was adopted in which site 1 was fully occupied with Bi and site 2 occupied with Sn. This model has the monoclinic base-centered lattice. The calculated electronic band structure and the DOS of

this model are presented in Figure 11. According to the results the electronic transitions from the VB to the CB are essentially direct but there is no single maximum or minimum, instead several flat bands between Y and L comprise the VBM and CBM. This is a peculiar band structure suggesting a possibility of a Fermi surface nesting upon doping (also between Z and Γ).

Despite a very different crystal structure, the electronic structure of Sn_2BiSI_5 maintains many features found in $Sn_2BiS_2I_3$. The VBM consist of strongly hybridized Sn *s*, S *p* and I *p* states, while the CBM is mainly made of fully hybridized Bi *p* and I *p* states. Therefore, it can be suggested that the BiI_6 octahedra of the extended BiI_3 ribbons have a significant contribution to the electronic structure and are responsible for the widening of the bandgap.

CONCLUDING REMARKS

The novel $Pb_2BiS_2I_3$, $Sn_2BiS_2I_3$ and Sn_2BiSI_5 can be synthesized by reacting a mixture of *M*S (M=Pb or Sn) and BiI_3, as well as their respective elements. $Pb_2BiS_2I_3$ and $Sn_2BiS_2I_3$ are isostructural and the Sn_2BiSI_5 can be considered as their homologue. These thioidodies are highly resistive n-type direct band gap semiconductors. The band structure calculations of these compounds show that the valence band mainly consist of iodine *p* orbital whereas conduction band is attributed mainly by a combination of Bi and iodine orbitals. $Pb_2BiS_2I_3$, $Sn_2BiS_2I_3$ and Sn_2BiSI_5 are stable in air, water and exhibit bandgaps between 1.2 to 1.6 eV making them interesting for solar cell applications. $Pb_2BiS_2I_3$, and $Pb_2SbS_2I_3$, consist of atoms with high atomic number, ($Z \geq 40$), and possess high mass density, high electrical resistivity and wide optical band gap ($1.5 \leq E_g \leq 2.0$), and therefore could be interesting for further research as room temperature nuclear radiation detection.

NOTE: Authors declare no competing financial interest.

ASSOCIATED CONTENT

*Supporting Information

Details on the DTA and TGA as well as EDS analysis of the thioiodides, thermal conductivity and Seebeck plots are given. X-ray crystallographic file (CIF), crystallographic refinement details, atomic coordinates with equivalent isotropic displacement parameters, anisotropic displacement parameters, and details bond distances and angles for $Pb_2BiS_2I_3$, $Sn_2BiS_2I_3$ and Sn_2BiSI_5. This material is available free of charge via the Internet at http://pubs.acs.org.

AUTHOR INFORMATION

Corresponding Author

*E-mail: m-kanatzidis@northwestern.edu

Author Contributions

The manuscript was written through contributions of all authors. All authors have given approval to the final version of the manuscript.

ACKNOWLEDGEMENTS

DJ and MSI acknowledge partial support from NSF grant DMR-1410169 and OYK and AJF (electrical measurements) are supported by DHS-ARI grant 2014-DN-077-ARI086-01. We also MRSEC program (NSF DMR-1121262) at the Materials Research Center for use of facilities. SEM, EDS and XPS analyses were performed at the EPIC facility of the NUANCE Center at Northwestern University, supported by NSF-NSEC, NSF-MRSEC, Keck Foundation, the State of Illinois, and Northwestern University.

Table 1 Details concerning data collection and structure refinement of $Pb_2BiS_2I_3$, $Sn_2BiS_2I_3$ and Sn_2BiSI_5.

Crystal data			
compounds	$Pb_2BiS_2I_3$	$Sn_2BiS_2I_3$	Sn_2BiSI_5
Molecular weight, M_r	1069.97	891.18	1112.92
Crystal system	Orthorhombic	Orthorhombic	Monoclinic
space group	*Cmcm*	*Cmcm*	*C*2/*m*
Temperature (K)	293	293	293
a (Å)	4.3214 (9)	4.2890 (6)	14.175 (3)
b (Å)	14.258 (3)	14.121 (2)	4.3985 (9)
c (Å)	16.488 (3)	16.414 (3)	21.625 (4)
β (°)	90.0	90.0	98.90 (3)
V (Å^3)	1015.9 (4)	994.1 (3)	1332.1 (5)
Z	4	4	4
Radiation type	Mo *K*α	Mo *K*α	Mo *K*α
μ (mm^{-1})	60.54	32.30	28.59
Crystal size (mm)	0.02 × 0.01 × 0.01	0.02 × 0.02 × 0.01	0.13 × 0.02 × 0.01
Data collection			
Diffractometer	STOE *IPDS* 2T	STOE *IPDS* 2T	STOE *IPDS* 2
*Θ*max; *θ*min	25.0°; 2.9°	29.1°; 3.1°	25.0°, 1.9°
Measured hkl	*h* = −5→5	*h* = −5→5	*h* = −16→16
	k = 0→16	*k* = −19→19	*k* = −5→5
	l = 0→19	*l* = −22→22	*l* = 0→25
Absorption correction	numerical	numerical	numerical
T_{min}, T_{max}	0.930, 0.941	0.503, 0.657	0.507, 0.757
No. of measured, independent and observed reflections	883, 531, 474	4225, 763, 653	2323, 1342, 1001
R_{int}	0.020	0.094	0.040
$(\sin\theta/\lambda)_{max}$ (Å^{-1})	0.594	0.685	0.594
Refinement			
R_1	0.022	0.053	0.046
wR_2	0.054	0.123	0.109
S	1.02	1.09	1.01
No. of reflections	531	763	1342
No. of parameters	28	29	57
$\Delta\rho_{max}$, $\Delta\rho_{min}$ (e Å^{-3})	1.09, −1.43	5.93, −4.51	2.06, −1.92

[a] $R_1 = \Sigma||F_o| - |F_c|| / |F_o|$, $F_o^2 \geq 2\sigma(F_o^2)$

[b] $wR_2 = 1 / [\sigma^2(F_o^2) + (A \cdot P)^2 + B \cdot P]$; $P = (F_o^2 + 2F_c^2) / 3$

Table 2: Atomic coordinates and isotropic displacement parameters for $M_2BiS_2I_3$ (*M* = Pb, Sn) and Sn_2BiSI_5.

compounds	Atom	Wyck.	S.O.F	x/a	y/b	z/c	U [Å^2]
$Pb_2BiS_2I_3$	Pb1	8f	0.5	1/2	0.36655(4)	0.02786(3)	0.0297(2)
	Bi1	8f	0.5	1/2	0.36655(4)	0.02786(3)	0.0297(2)
	Pb2	4c	1.0	0	0.19051(6)	1/4	0.0399(4)
	I1	4c	1.0	-1/2	0.34973(8)	1/4	0.0197(3)
	I2	8f	1.0	1/2	0.05475(6)	0.12070(5)	0.0215(3)
	S1	8f	1.0	0	0.2672(2)	0.08268(17)	0.0185(6)
$Sn_2BiS_2I_3$	Sn1	4*c*	1.0	0	0.2971 (2)	1/4	0.064 (1)
	Bi1	8*f*	0.506 (13)	1/2	0.13382 (7)	0.02054 (7)	0.0291 (4)
	Sn2	8f	0.494 (13	1/2	0.13382 (7)	0.02054 (7)	0.0291 (4)
	I1	8f	1.0	1/2	0.44358 (9)	0.12166 (7)	0.0227 (4)
	I2	4c	1.0	1/2	0.1456 (1)	1/4	0.0234 (5)
	S1	8f	1.0	1/2	0.2707 (3)	−0.0819 (2)	0.0179 (8)
Sn_2BiSI_5	Bi1A	4i	0.763 (14)	0.25718 (8)	0	0.09971 (5)	0.0426 (5)
	Sn1A	4i	0.237 (14)	0.25718 (8)	0	0.09971 (5)	0.0426 (5)
	Bi2A	4i	0.228 (14)	0.1274(1)	0	0.47820 (7)	0.0455 (7)
	Sn2A	4i	0.772 (14)	0.1274 (1)	0	0.47820 (7)	0.0455 (7)
	Sn3	4i	1.0	0.2379 (1)	0	0.67635 (9)	0.0471 (5)
	S1	4i	1.0	0.2848 (4)	0	0.5611 (3)	0.036 (1)
	I1	4i	1.0	0.1257 (1)	−1/2	0.13935 (9)	0.0506 (5)
	I2	4i	1.0	0.4204 (1)	0	0.40632 (7)	0.0375 (4)
	I3	4i	1.0	0.39160 (1)	−1/2	0.69695 (7)	0.0406 (4)
	I4	4i	1.0	0.3847 (1)	−1/2	0.04602 (8)	0.0458 (5)
	I5	4i	1.0	0.3792 (1)	0	0.21971 (7)	0.0454 (4)

Table 3 : Anisotropic displacement parameters (Å^2) for X, Y and Z…

compounds	*atoms*	U^{11}	U^{22}	U^{33}	U^{12}	U^{13}	U^{23}
	Pb1	0.0244(3)	0.0330(3)	0.0316(3)	0	0	0.0068(2)
	Bi1	0.0244(3)	0.0330(3)	0.0316(3)	0	0	0.0068(2)
$Pb_2BiS_2I_3$	Pb2	0.0269(5)	0.0339(5)	0.0590(6)	0	0	0
	I1	0.0185(6)	0.0230(6)	0.0172(5)	0	0	0
	I2	0.0210(4)	0.0218(4)	0.0216(4)	0	0	0.0019(3)
	S1	0.0219(15)	0.0194(15)	0.0140(13)	0	0	0.0002(12)
	Sn1	0.0311 (13)	0.035 (2)	0.125 (3)	0	0	0
	Bi1	0.0321 (6)	0.0244 (6)	0.0308 (6)	0	0	0.0012 (4)
$Sn_2BiS_2I_3$	Sn2	0.0321 (6)	0.0244 (6)	0.0308 (6)	0	0	0.0012 (4)
	I1	0.0233 (6)	0.0244 (7)	0.0204 (6)	0	0	−0.0033 (4)
	I2	0.0212 (9)	0.029 (1)	0.0198 (7)	0	0	0
	S1	0.020 (2)	0.021 (2)	0.012 (2)	0	0	−0.002 (2)
	Bi1A	0.0520 (8)	0.0399 (7)	0.0374 (7)	0	0.0114 (5)	0
	Sn1A	0.0520 (8)	0.0399 (7)	0.0374 (7)	0	0.0114 (5)	0
	Bi2A	0.046 (1)	0.039 (1)	0.054 (1)	0	0.0151 (7)	0
	Sn2A	0.046 (1)	0.039 (1)	0.054 (1)	0	0.0151 (7)	0
Sn_2BiSI_5	Sn3	0.060 (1)	0.0369 (9)	0.048 (1)	0	0.0190 (9)	0
	S1	0.047 (3)	0.029 (3)	0.034 (3)	0	0.012 (2)	0
	I1	0.050 (1)	0.043 (1)	0.064 (1)	0	0.0242 (8)	0
	I2	0.0414 (9)	0.0324 (8)	0.0403 (8)	0	0.0115 (7)	0
	I3	0.0458 (9)	0.0308 (8)	0.0454 (9)	0	0.0080 (7)	0
	I4	0.0494 (1)	0.0429 (9)	0.0483 (9)	0	0.0173 (7)	0
	I5	0.0522 (1)	0.0463 (9)	0.0384 (8)	0	0.0090 (7)	0

Table 4: Selected interatomic distances (Å) and angles (°) in $Pb_2BiS_2I_3$; estimated standard deviation in parentheses.

Pb1|Bi1—S1^{i}	2.638(3)	I1—Pb2^{ix}	3.1342(11)
Pb1|Bi1—S1	2.7372(19)	I1—Pb1|Bi1^{x}	3.6705(9)
Pb1|Bi1—S1^{ii}	2.7372(19)	I1—Pb1|Bi1^{x}	3.6705(9)
Pb1|Bi1—I2^{i}	3.4535(8)	I1—Pb1|Bi1^{ix}	3.6705(9)
Pb1|Bi1—I2^{iii}	3.4535(8)	I1—Pb1|Bi1^{ix}	3.6705(9)
Pb1|Bi1—I1^{ii}	3.6705(9)	I2—Pb1|Bi1^{i}	3.4535(8)
Pb1|Bi1—I2^{iv}	3.7699(9)	I2—Pb1|Bi1^{i}	3.4535(8)
Pb1|Bi1—I2^{v}	3.7699(9)	I2—Pb1|Bi1^{iii}	3.4535(8)
Pb2—S1^{vii}	2.968(3)	I2—Pb1|Bi1^{xii}	3.7699(9)
Pb2—S1	2.968(3)	S1—Pb1|Bi1^{i}	2.638(3)
Pb2—I1^{ii}	3.1341(11)	S1—Pb1|Bi1^{i}	2.638(3)
Pb2—I1	3.1342(11)	S1—Pb1|Bi1^{ix}	2.7372(19)
Pb2—S1^{vii}	2.968(3)	I2—Pb1|Bi1^{xii}	3.7699(9)
Pb2—S1	2.968(3)	S1—Pb1|Bi1^{i}	2.638(3)
S1^{vii}—Pb2—S1	136.75(12)	Pb1|Bi1^{i}—S1—Pb1|Bi1^{ix}	98.40(8)
S1^{vii}—Pb2—I1^{ii}	74.52(4)	Pb1|Bi1^{i}—S1—Pb1|Bi1^{ix}	98.40(8)
S1—Pb2—I1^{ii}	74.52(4)	Pb1|Bi1—S1—Pb1|Bi1^{ix}	104.300
S1^{vii}—Pb2—I1	74.52(4)	Pb1|Bi1^{i}—S1—Pb1|Bi1^{ix}	98.400
S1—Pb2—I1	74.52(4)	Pb1|Bi1^{i}—S1—Pb1|Bi1^{ix}	98.40(8)
I1^{ii}—Pb2—I1	87.17(4)	Pb1|Bi1—S1—Pb1|Bi1^{ix}	104.26(10)

Symmetry codes: (i) −x+1/2, −y+1/2, −z; (ii) x+1, y, z; (iii) x, y, −z+1/2; (iv) x−1, y, z.

Table 5: Selected interatomic distances (Å) and angles (°) in $Sn_2BiS_2I_3$; estimated standard deviation in parentheses.

Sn1—S1^{i}	2.921(4)	S1—Bi1|Sn2^{iv}	2.726(3)
Sn1—S1^{ii}	2.921(4)	S1—Bi1|Sn2^{iv}	2.726(3)
Sn1—I2^{iii}	3.030(2)	S1—Bi1|Sn2^{i}	2.726(3)
Sn1—I2	3.030(2)	S1—Bi1|Sn2^{i}	2.726(3)
Bi1|Sn2—S1	2.562(4)	S1—Sn1^{i}	2.921(4)
Bi1|Sn2—S1^{iv}	2.726(3)	Sn1—I1^{iii}	3.6490(19)
Bi1|Sn2—S1^{i}	2.726(3)	Sn1—S1^{vi}	2.9206(36)
Bi1|Sn2—I1^{i}	3.3527(13)	Bi1|Sn2—I1^{vii}	3.8171(14)
Bi1|Sn2—I1^{iv}	3.3527(13)	Bi1|Sn2—I1^{viii}	3.3528(13)
S1^{i}—Sn1—S1^{ii}	141.7(2)	Sn1^{v}—I2—Sn1	90.11(9)
S1^{i}—Sn1—I2^{iii}	76.61(7)	Bi1|Sn2—S1—Bi1|Sn2^{iv}	97.500
S1^{ii}—Sn1—I2^{iii}	76.61(7)	Bi1|Sn2—S1—Bi1|Sn2^{iv}	97.52(10)
S1^{i}—Sn1—I2	76.61(7)	Bi1|Sn2^{iv}—S1—Bi1|Sn2^{iv}	0.000
S1^{ii}—Sn1—I2	76.61(7)	Bi1|Sn2—S1—Bi1|Sn2^{i}	97.500
I2^{iii}—Sn1—I2	90.11(9)	Bi1|Sn2^{iv}—S1—Bi1|Sn2^{i}	103.76(15)
S1—Bi1|Sn2—S1^{iv}	82.47(10)	Bi1|Sn2^{iv}—S1—Bi1|Sn2^{i}	103.76(15)
S1—Bi1|Sn2—S1^{i}	82.47(10)	Bi1|Sn2—S1—Bi1|Sn2^{i}	97.52(10)
S1^{iv}—Bi1|Sn2—S1^{i}	103.76(15)	Bi1|Sn2^{iv}—S1—Bi1|Sn2^{i}	103.800
S1—Bi1|Sn2—I1^{i}	77.83(8)	Bi1|Sn2^{iv}—S1—Bi1|Sn2^{i}	103.76(15)
S1^{i}—Sn1—S1^{ii}	141.7(2)	Sn1^{v}—I2—Sn1	90.11(9)
S1^{i}—Sn1—I2^{iii}	76.61(7)	Bi1|Sn2—S1—Bi1|Sn2^{iv}	97.500
S1^{ii}—Sn1—I2^{iii}	76.61(7)	Bi1|Sn2—S1—Bi1|Sn2^{iv}	97.52(10)
S1^{i}—Sn1—I2	76.61(7)	Bi1|Sn2^{iv}—S1—Bi1|Sn2^{iv}	0.000
S1^{ii}—Sn1—I2	76.61(7)	Bi1|Sn2—S1—Bi1|Sn2^{i}	97.500

Symmetry codes: (i) –x+1/2, -y+1/2, -z; (ii) –x+1/2, -y+1/2, z+1/2; (iii) x-1, y, z; (iv) –x+3/2, -y+1/2, -z; (v) x+1, y, z;

Table 6: Selected interatomic distances (Å) and angles (°) in Sn_2BiSI_5; estimated standard deviation in parentheses.

Bi1A—I5	2.888 (2)	Sn3—I3^{i}	3.0791 (19)
Bi1A—I1^{i}	3.0881 (15)	S1—Sn2A^{ii}	2.727 (3)
Bi1A—I1	3.0882 (15)	S1—Bi2A^{ii}	2.727 (3)
Bi1A—I4	3.1780 (15)	S1—Bi2A^{iii}	2.727 (3)
Bi1A—I4^{i}	3.1781 (15)	S1—Sn2A^{iii}	2.727 (3)
Bi2A—S1	2.638 (7)	I1—Sn1A^{iv}	3.0882 (15)
Bi2A—S1^{ii}	2.727 (3)	I1—Bi1A^{iv}	3.0882 (15)
Bi2A—S1^{iii}	2.727 (3)	I3—Sn3^{iv}	3.0791 (19)
Sn3—S1	2.676 (6)	I4—Sn1A^{iv}	3.1780 (15)
Sn3—I3	3.0791 (19)	I4—Bi1A^{iv}	3.1780 (15)
I5—Bi1A—I1^{i}	93.08 (5)	Bi2A—S1—Bi2A^{ii}	99.61 (15)
I5—Bi1A—I1	93.08 (5)	Sn3—S1—Bi2A^{ii}	118.78 (13)
I1^{i}—Bi1A—I1	90.82 (5)	Bi2A—S1—Bi2A^{iii}	99.61 (15)
I5—Bi1A—I4	91.88 (5)	Sn3—S1—Bi2A^{iii}	118.78 (13)
I1^{i}—Bi1A—I4	174.76 (6)	Sn2A^{ii}—S1—Bi2A^{iii}	107.5
I1—Bi1A—I4	90.58 (3)	Bi2A^{ii}—S1—Bi2A^{iii}	107.49 (19)
I5—Bi1A—I4^{i}	91.89 (5)	Bi2A—S1—Sn2A^{iii}	99.6(4)
I1^{i}—Bi1A—I4^{i}	90.58 (4)	Sn3—S1—Sn2A^{iii}	118.78 (13)
I1—Bi1A—I4^{i}	174.76 (6)	Sn2A^{ii}—S1—Sn2A^{iii}	107.49 (19)
I4—Bi1A—I4^{i}	87.58 (5)	Bi2A^{ii}—S1—Sn2A^{iii}	107.49 (19)
S1—Bi2A—S1^{ii}	80.39 (15)	Bi2A^{iii}—S1—Sn2A^{iii}	0.00 (6)
S1—Bi2A—S1^{iii}	80.39 (15)	Bi1A—I1—Sn1A^{iv}	90.8(2)
S1^{ii}—Bi2A—S1^{iii}	107.49 (19)	Bi1A—I1—Bi1A^{i}	90.82 (6)
S1—Sn3—I3	82.11 (11)	Sn3—I3—Sn3^{iv}	91.16 (7)
S1—Sn3—I3^{i}	82.11 (11)	Sn1A^{iv}—I4—Bi1A	87.6(6)
I3—Sn3—I3^{i}	91.16 (7)	Bi1A^{iv}—I4—Bi1A	87.58 (5)
Bi2A—S1—Sn3	109.1 (2)	Sn3—S1—Sn2A^{ii}	118.78 (13)
Bi2A—S1—Sn2A^{ii}	99.6(3)		

Symmetry codes: (i) x, y+1, z; (ii) –x+1/2, -y+1/2, -z+1; (iii) –x+1/2, -y-1/2, -z+1; (iv) x. y-1, z.

Table 7: Binding energies of $Pb_2BiS_2I_3$, $Sn_2BiS_2I_3$ and Sn_2BiSI_5 obtained from XPS spectra

Compounds	Binding energy (eV)	assignment	Spin-orbit components (eV)	References
$Pb_2BiS_2I_3$	143.34	Pb $4f_{5/2}$	ΔPb $4f$ = 4.91	53
	138.43	Pb $4f_{7/2}$		
	158.90	Bi $4f_{7/2}$	ΔBi $4f$ = 5.31	53
	164.21	Bi $4f_{5/2}$		
	619.63	I $3d_{5/2}$	ΔI $3d$ = 11.44	53
	631.07	I $3d_{3/2}$		
	161.84	S $2p$	------	59-60
	225.64	S $2s$	------	
$Sn_2BiS_2I_3$	486.73	Sn $3d_{5/2}$	ΔSn $3d$ = 8.39	53-54
	495.12	Sn $3d_{3/2}$		
	158.82	Bi $4f_{7/2}$	ΔBi $4f$ = 5.28	53
	164.10	Bi $4f_{5/2}$		
	619.32	I $3d_{5/2}$	ΔI $3d$ = 11.46	53
	630.78	I $3d_{3/2}$		
	161.70	S $2p$	------	53, 59
	225.92	S $2s$	------	
Sn_2BiSI_5	487.34	Sn $3d_{3/2}$	ΔSn $3d$ = 8.42	54
	495.76	Sn $3d_{5/2}$		
	159.12	Bi $4f_{7/2}$	ΔBi $4f$ = 5.29	53
	164.41	Bi $4f_{5/2}$		
	619.68	I $3d_{5/2}$	ΔI $3d$ = 11.48	53
	631.16	I $3d_{3/2}$		
	162.10	S $2p$	------	53, 59
	225.97	S $2s$	------	

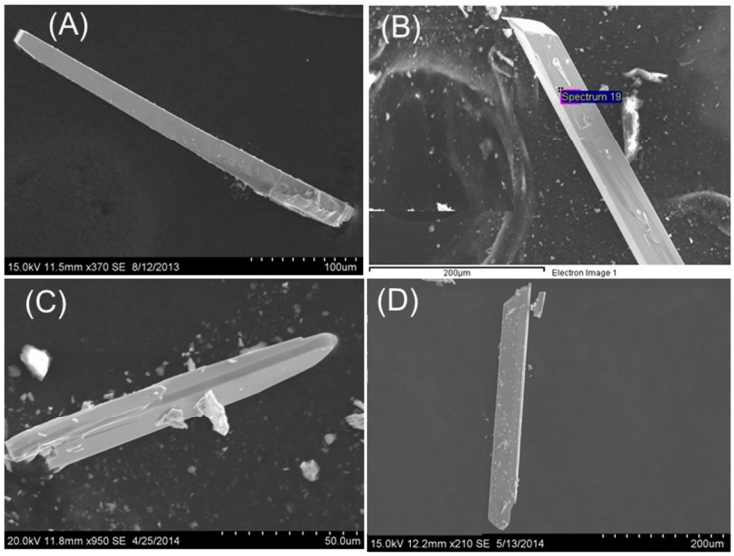

Figure 1: SEM images of (A) $Pb_2BiS_2I_3$, (B) "$Pb_2Sb_{1-x}Bi_xS_2I_3$" (x~0.4), (C) $Sn_2BiS_2I_3$, and (D) Sn_2BiSI_5 showing the characteristics growth of the crystal along *c*-axis.

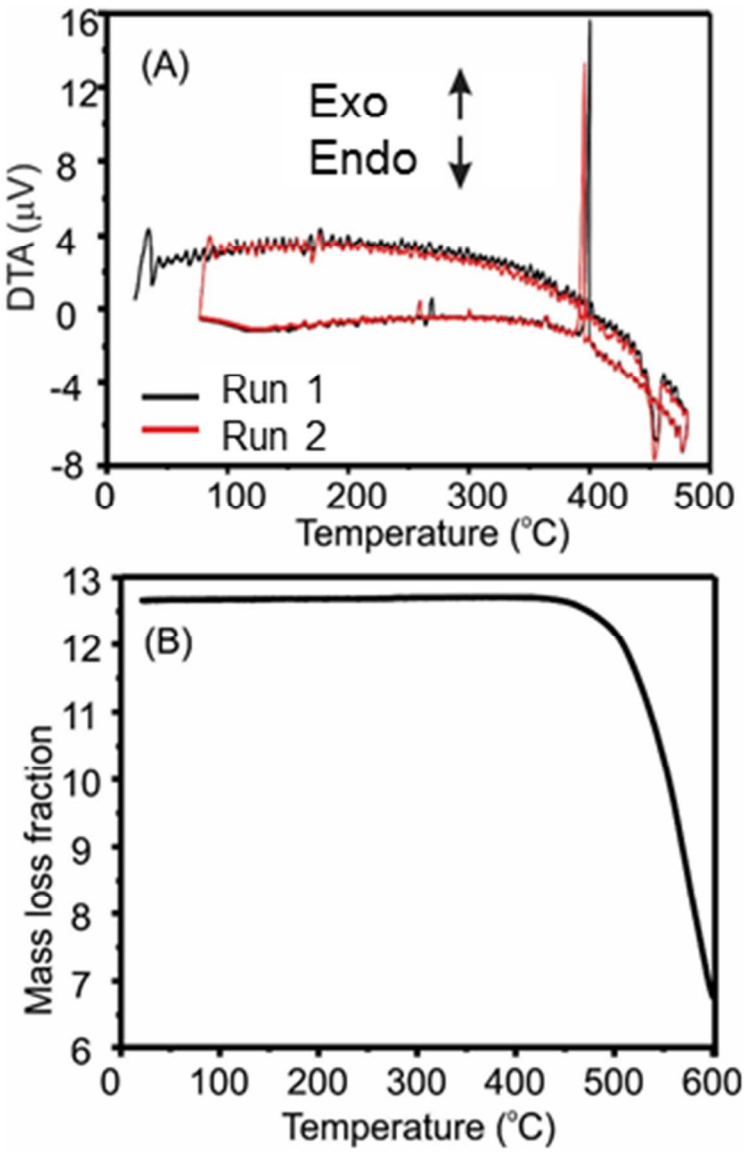

Figure 2. (A) Differential thermal analysis (5deg/min) and (B) Thermogravimetric analysis a sample of $Pb_2BiS_2I_3$ (10 deg/min).

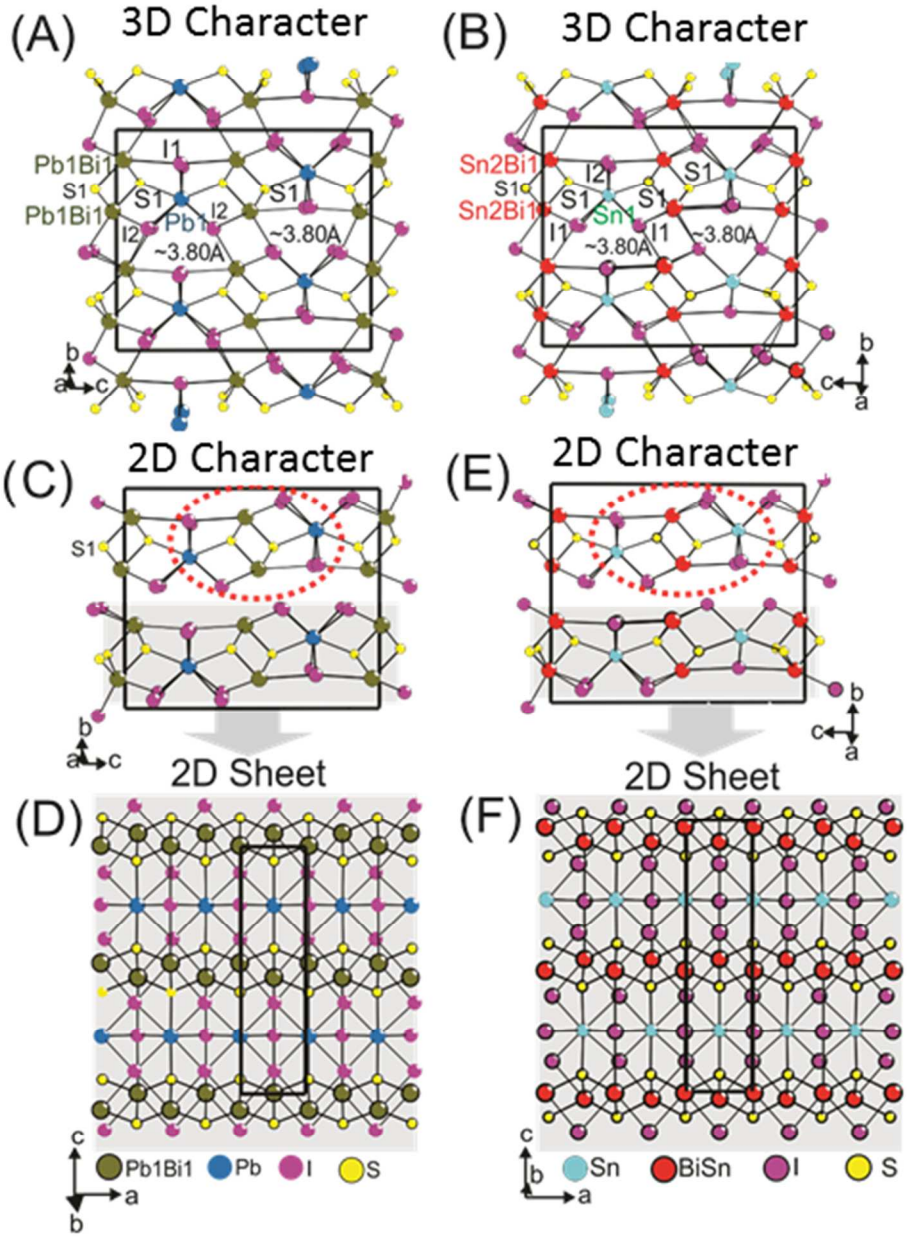

Figure 3: Crystal structures of (A, C, D) $Pb_2BiS_2I_3$, and (B, E, F) $Sn_2BiS_2I_3$. Figures C and E represent the infinite ribbon $[M_4S_2I_4]$ (M = Pb, Sn, Bi) running along c-axis, red circles indicate the isolated ribbon. D and F derived from grey shaded region of the ribbons (C and E) clearly show the 2D sheet.

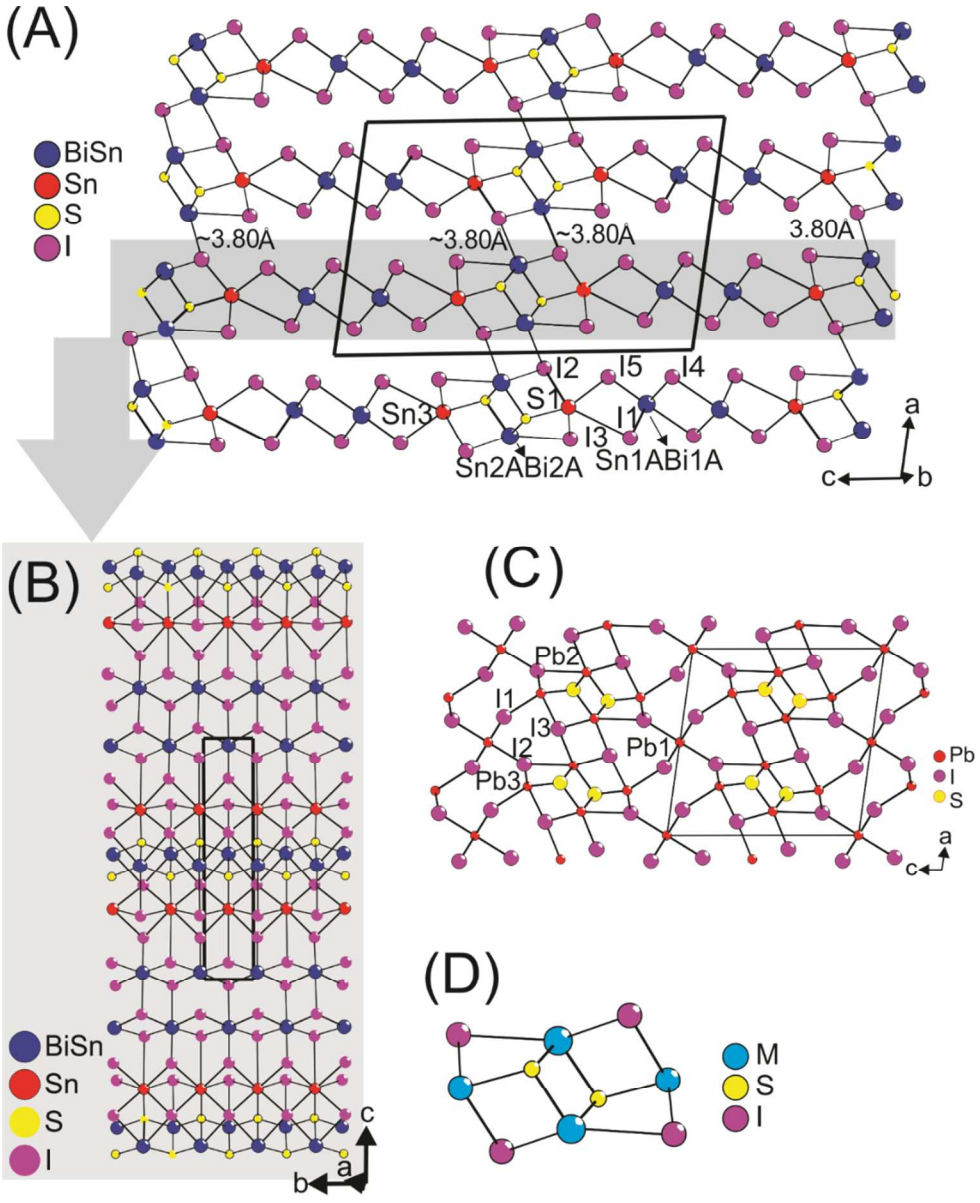

Figure 4. Crystal structures of new (A) Sn_2BiSI_5, and known (B) $Pb_5S_2I_6$.[50] Figure (B) is isolated 2D view of the crystal structures derived from grey shaded region of the crystal structure A. Figure (D) represents the common structural fragment $[M_4S_2I_4]$ (M = Pb, Bi, Sn).

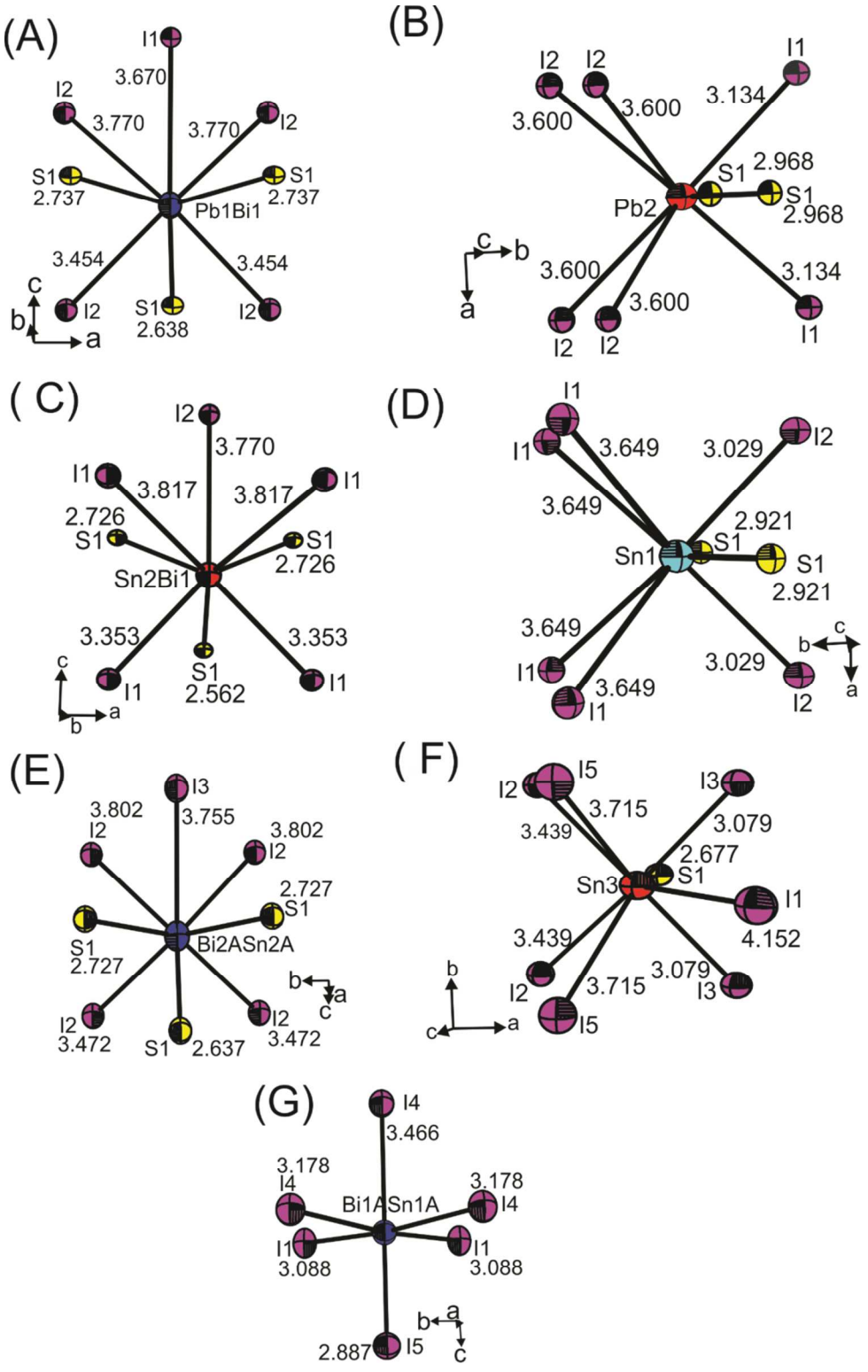

Figure 5: Coordination polyhedral representations of (A, B) $Pb_2BiS_2I_3$, (C, D) $Sn_2BiS_2I_3$, (E, F) Sn_2BiSI_5. Ellipsoids are at 50% probability levels.

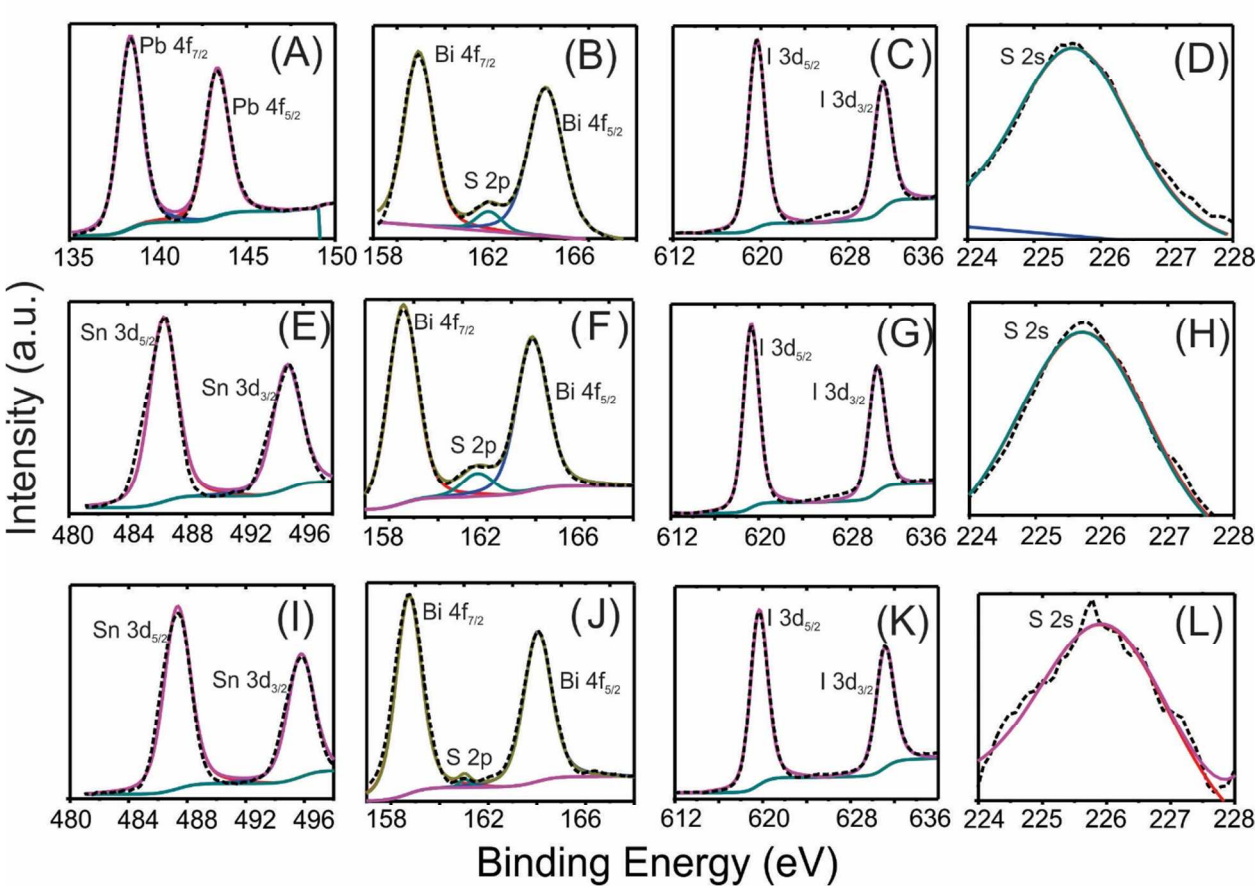

Figure 6: X-ray Photoelectron spectra of (A -D) $Pb_2BiS_2I_3$, (E-H) $Sn_2BiS_2I_3$, (I-L) Sn_2BiSI_5. (A) represents the binding energy of Pb 4f; (E,I) represent the binding energy of Sn 3d; (B,F, J) are denoted for Bi 4f and (D, H, L) are the characteristics of I 3d energies. Weak peaks at about 162 eV in (B, E, H) are due to S 2p energies. Dashed and solid lines represent experimental and calculated data, respectively.

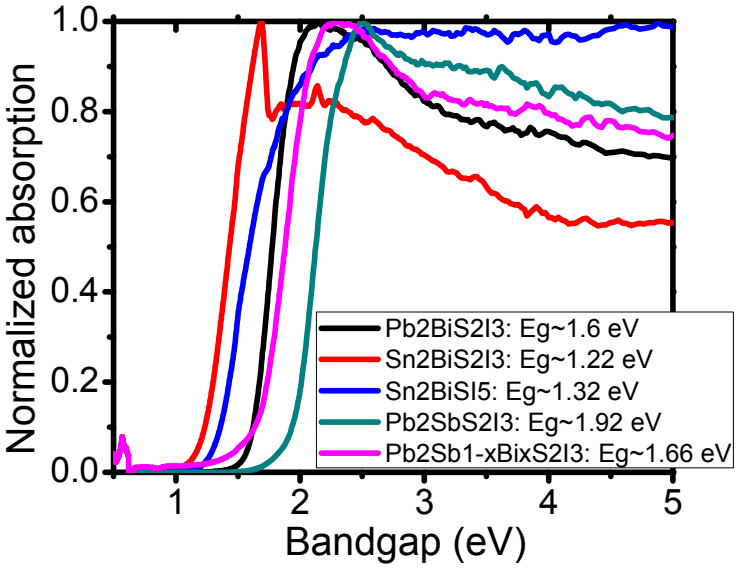

Figure 7. UV/Vis absorption spectrum of polycrystalline powder of $Pb_2BiS_2I_3$, $Sn_2BiS_2I_3$, $Pb_2SbS_2I_3$, "$Pb_2Sb_{1-x}Bi_xS_2I_3$" (x~0.4), and Sn_2BiSI_5. The bump at ~ 1.5 eV in red spectrum ($Sn_2BiS_2I_3$) is due to the detector switch which we see frequently to different samples.

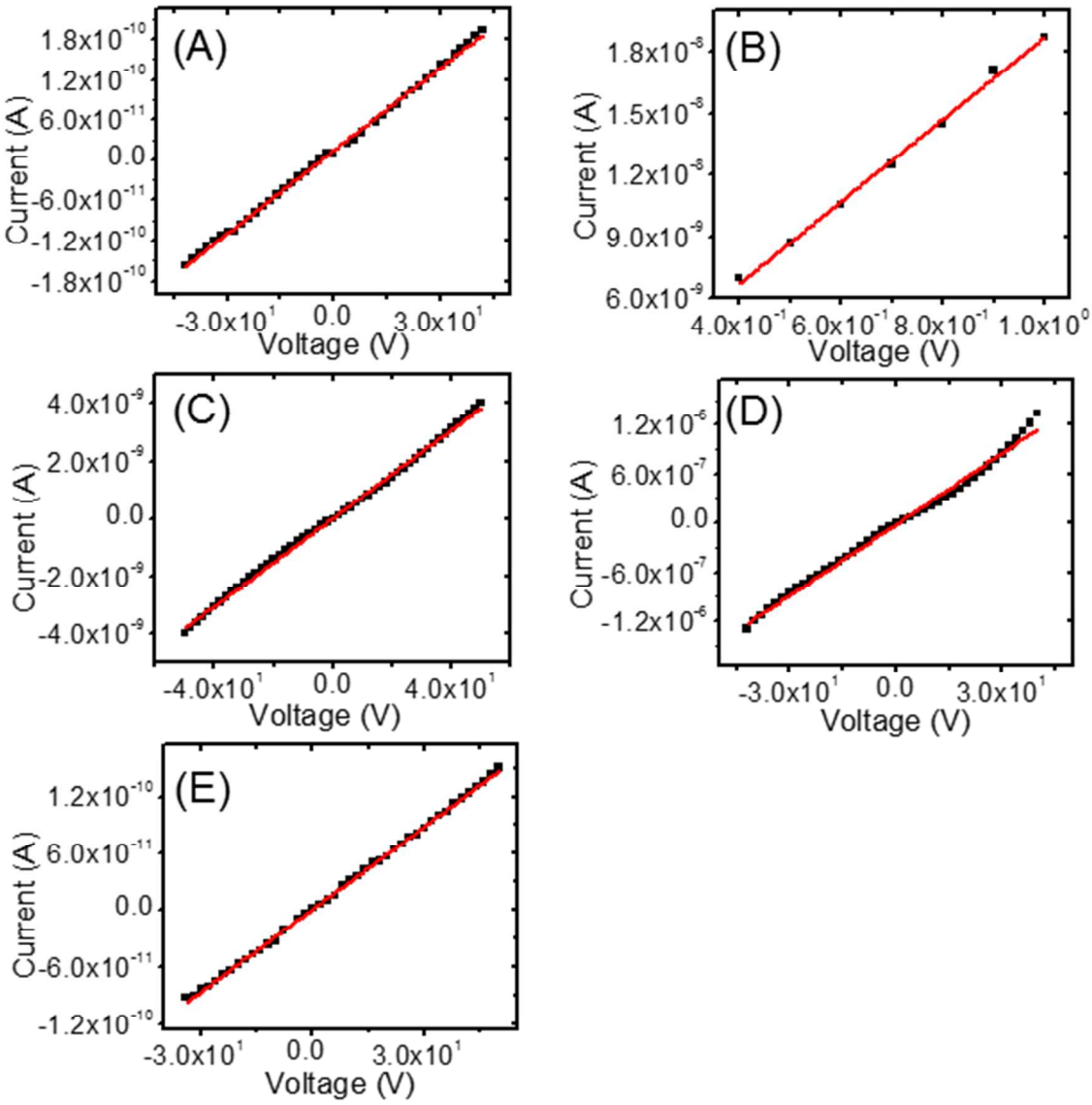

Figure 8. Electrical resistivity of (A) $Pb_2SbS_2I_3$, (B) $Pb_2BiS_2I_3$, (C) "$Pb_2Sb_{1-x}Bi_xS_2I_3$" (x~0.4), (D) $Sn_2BiS_2I_3$, and (E) Sn_2BiSI_5.

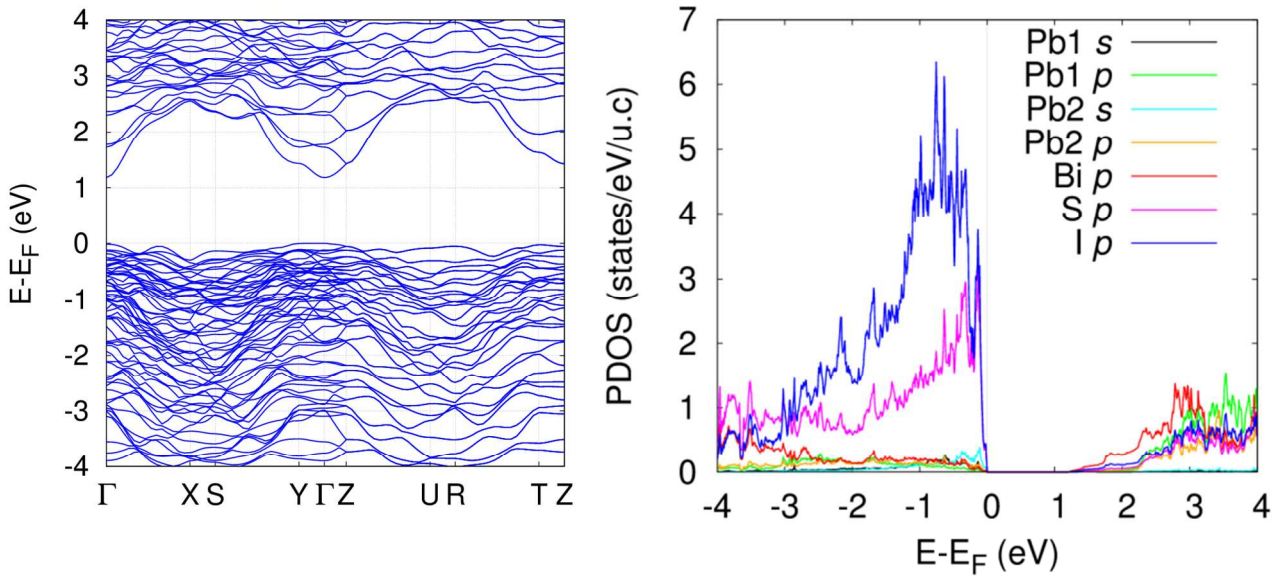

Figure 9. (A) Electronic band structure and (B) projected electronic density of states of $Pb_2BiS_2I_3$.

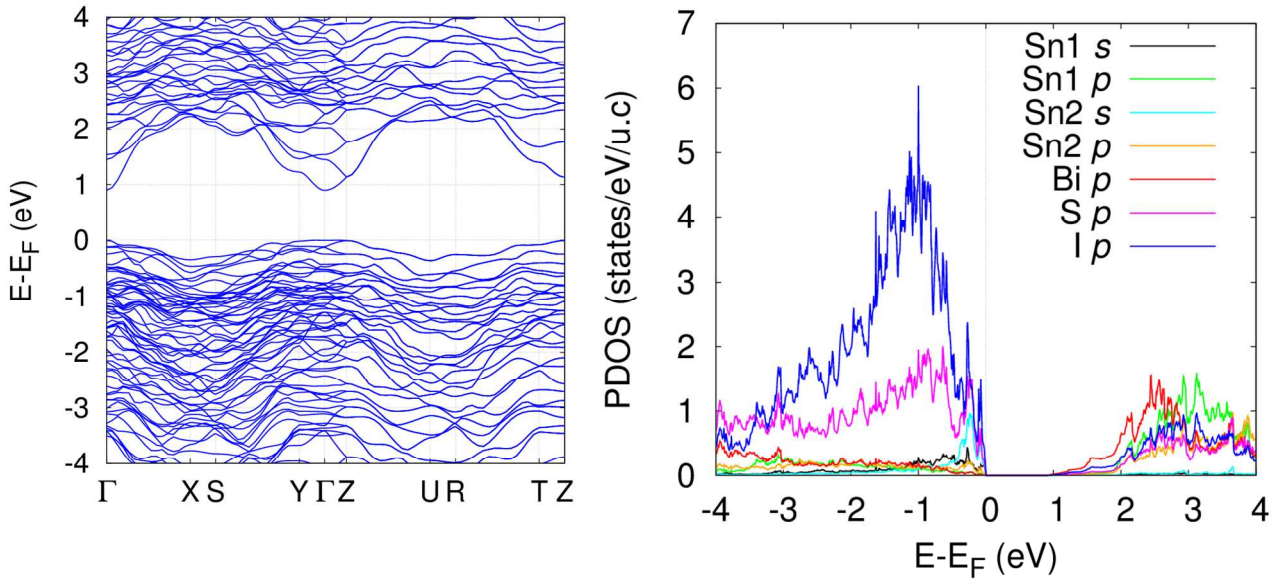

Figure 10. (A) Electronic band structure and (B) projected electronic density of states of $Sn_2BiS_2I_3$.

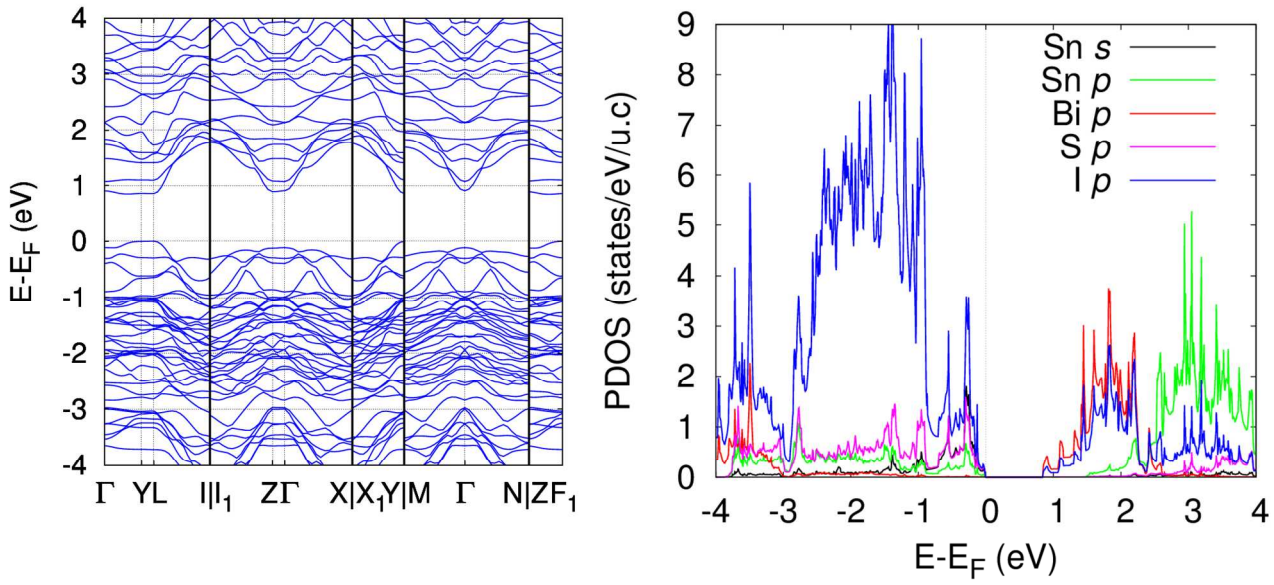

Figure 11. (A) Electronic band structure and (B) projected electronic density of states of Sn_2BiSI_5.

REFERENCES

1. Lee, W. L.; Watauchi, S.; Miller, V. L.; Cava, R. J.; Ong, N. P. Dissipationless anomalous Hall current in the ferromagnetic spinel $CuCr_2Se_{4-x}Br_x$. *Science* **2004**, *303*, 1647-9.
2. Yu, P.; Zhou, L. J.; Chen, L. Noncentrosymmetric inorganic open-framework chalcohalides with strong middle IR SHG and red emission: $Ba_3AGa_5Se_{10}Cl_2$ (A = Cs, Rb, K). *J. Am. Chem. Soc.* **2012**, *134*, 2227-35.
3. de la Cruz, C.; Huang, Q.; Lynn, J. W.; Li, J.; Ratcliff, W., 2nd; Zarestky, J. L.; Mook, H. A.; Chen, G. F.; Luo, J. L.; Wang, N. L.; Dai, P. Magnetic order close to superconductivity in the iron-based layered $LaO_{1-x}F_xFeAs$ systems. *Nature* **2008**, *453*, 899-902.
4. Zhao, J.; Huang, Q.; de la Cruz, C.; Li, S.; Lynn, J. W.; Chen, Y.; Green, M. A.; Chen, G. F.; Li, G.; Li, Z.; Luo, J. L.; Wang, N. L.; Dai, P. Structural and magnetic phase diagram of $CeFeAsO_{1-x}F_x$ and its relation to high-temperature superconductivity. *Nat. Mater.* **2008**, *7*, 953-9.
5. Johnsen, S.; Liu, Z.; Peters, J. A.; Song, J. H.; Nguyen, S.; Malliakas, C. D.; Jin, H.; Freeman, A. J.; Wessels, B. W.; Kanatzidis, M. G. Thallium chalcohalides for X-ray and gamma-ray detection. *J. Am. Chem. Soc.* **2011**, *133*, 10030-3.
6. Jiang, X. M.; Zhang, M. J.; Zeng, H. Y.; Guo, G. C.; Huang, J. S. Inorganic supramolecular compounds with 3-D chiral frameworks show potential as both mid-IR second-order nonlinear optical and piezoelectric materials. *J. Am. Chem. Soc.* **2011**, *133*, 3410-8.
7. Islam, S. M.; Subrahmanyam, K. S.; Malliakas, C. D.; Kanatzidis, M. G. One-Dimensional Molybdenum Thiochlorides and Their Use in High Surface Area MoS_x Chalcogels. *Chem. Mater.* **2014**, *26*, 5151-5160.
8. Wibowo, A. C.; Malliakas, C. D.; Liu, Z.; Peters, J. A.; Sebastian, M.; Chung, D. Y.; Wessels, B. W.; Kanatzidis, M. G. Photoconductivity in the chalcohalide semiconductor, SbSeI: a new candidate for hard radiation detection. *Inorg. Chem.* **2013**, *52*, 7045-50.
9. Li, Y. Y.; Wang, J. S.; Liu, B.; Dang, L. Y.; Yao, H. C.; Li, Z. J. BiOI-sensitized TiO_2 in phenol degradation: A novel efficient semiconductor sensitizer. *Chem. Phys. Lett.* **2011**, *508*, 102-106.
10. Li, Y. Y.; Wang, J. S.; Yao, H. C.; Dang, L. Y.; Li, Z. J. Chemical etching preparation of $BiOI/Bi_2O_3$ heterostructures with enhanced photocatalytic activities. *Catal. Commun.* **2011**, *12*, 660-664.
11. Donakowski, M. D.; Gorne, A.; Vaughey, J. T.; Poeppelmeier, K. R. $AgNa(VO_2F_2)_2$: a trioxovanadium fluoride with unconventional electrochemical properties. *J. Am. Chem. Soc.* **2013**, *135*, 9898-906.
12. Kamihara, Y.; Hiramatsu, H.; Hirano, M.; Kawamura, R.; Yanagi, H.; Kamiya, T.; Hosono, H. Iron-based layered superconductor: LaOFeP. *J. Am. Chem. Soc.* **2006**, *128*, 10012-3.
13. Chen, X. H.; Wu, T.; Wu, G.; Liu, R. H.; Chen, H.; Fang, D. F. Superconductivity at 43 K in $SmFeAsO_{1-x}F_x$. *Nature* **2008**, *453*, 761-2.
14. Kamihara, Y.; Watanabe, T.; Hirano, M.; Hosono, H. Iron-based layered superconductor $La[O_{1-x}F_x]FeAs$ (x = 0.05-0.12) with T_c = 26 K. *J. Am. Chem. Soc.* **2008**, *130*, 3296-7.
15. Mazin, I. I.; Singh, D. J.; Johannes, M. D.; Du, M. H. Unconventional superconductivity with a sign reversal in the order parameter of $LaFeAsO_{1-x}F_x$. *Phys. Rev. Lett.* **2008**, *101*, 057003-4.
16. Kuroki, K.; Onari, S.; Arita, R.; Usui, H.; Tanaka, Y.; Kontani, H.; Aoki, H. Unconventional pairing originating from the disconnected Fermi surfaces of superconducting $LaFeAsO_{1-x}F_x$. *Phys. Rev. Lett.* **2008**, *101*, 087004-4.
17. Hiramatsu, H.; Kamioka, H.; Ueda, K.; Ohta, H.; Kamiya, T.; Hirano, M.; Hosono, H. Opto-electronic properties and light-emitting device application of widegap layered oxychalcogenides: LaCuOCh (Ch = chalcogen) and $La_2CdO_2Se_2$. *Phys. Status Solidi A* **2006**, *203*, 2800-2811.

18. Park, C. H.; Keszler, D. A.; Yanagi, H.; Tate, J. Gap modulation in $MCu[Q_{1-x}Q'_x]F$ (M = Ba, Sr; Q, Q ' = S, Se, Re) and related materials. *Thin Solid Films* **2003**, *445*, 288-293.
19. Yanagi, H.; Park, S.; Draeseke, A. D.; Keszler, D. A.; Tate, J. P-type conductivity in transparent oxides and sulfide fluorides. *J. Solid. State. Chem.* **2003**, *175*, 34-38.
20. Yanagi, H.; Tate, J.; Park, S.; Park, C. H.; Keszler, D. A. p-type conductivity in wide-band-gap BaCuQF (Q=S,Se). *Appl. Phys. Lett.* **2003**, *82*, 2814-2816.
21. Zhang, Q.; Chung, I.; Jang, J. I.; Ketterson, J. B.; Kanatzidis, M. G. Chalcogenide Chemistry in Ionic Liquids: Nonlinear Optical Wave-Mixing Properties of the Double-Cubane Compound $[Sb_7S_8Br_2](AlCl_4)_3$. *J. Am. Chem. Soc.* **2009**, *131*, 9896-9897.
22. Chung, I.; Kanatzidis, M. G. Metal Chalcogenides: A Rich Source of Nonlinear Optical Materials. *Chem. Mater.* **2014**, *26*, 849-869.
23. Doussier, C.; Leone, P.; Moelo, Y. Single crystal structure and magnetic properties of $MnSbS_2Cl$. *Solid State Sci.* **2004**, *6*, 1387-1391.
24. Tougait, O.; Ibers, J. A.; Mar, A. Manganese antimony diselenide iodide, $MnSbSe_2I$. *Acta Crystallogr. C* **2003**, *59*, I77-I78.
25. Baranov, A. I.; Kloo, L.; Olenev, A. V.; Popovkin, B. A.; Romanenko, A. I.; Shevelkov, A. V. Unique [^{1infinity}Ni8Bi8S] metallic wires in a novel quasi-1D compound. Synthesis, crystal and electronic structure, and properties of Ni_8Bi_8SI. *J. Am. Chem. Soc.* **2001**, *123*, 12375-9.
26. Sirota, M. I.; Simonov, M. A.; Egorovtismenko, Y. K.; Simonov, V. I.; Belov, N. V. Crystal-Structure of $CdSb_6S_8I_4$. *Kristallografiya* **1976**, *21*, 64-68.
27. Gout, D.; Jobic, S.; Evain, M.; Brec, R. New antimony lanthanide disulfide dibromides $LnSbS_2Br_2$ (Ln = La, Ce): Crystal and electronic structures and optical properties. *J. Solid State Chem.* **2001**, *158*, 218-226.
28. Gout, D.; Jobic, S.; Evain, M.; Brec, R. Synthesis, structure and optical properties of new lanthanide-based derivatives Ln_2SbS_5Br (Ln = La, Ce). *Solid State Sci.* **2001**, *3*, 223-234.
29. Gitzendanner, R. L.; DiSalvo, F. J. Synthesis and Structure of a New Quinary Sulfide Halide: $LaCa_2GeS_4Cl_3$. *Inorg. Chem.* **1996**, *35*, 2623-2626.
30. Mariolacos, K.; Kupcik, V. Crystal-Structure of $Bi_2Cu_3S_4Br$. *Acta Crystallogr. B* **1975**, *31*, 1762-1763.
31. Kabbour, H.; Cario, L. $Ae_2Sb_2X_4F_2$ (Ae = Sr, Ba): new members of the homologous series $Ae_2M_{1+n}X_{3+n}F_2$ designed from rock salt and fluorite 2D building blocks. *Inorg. Chem.* **2006**, *45*, 2713-7.
32. Kramer, V. Vapor Growth and Structural Characterization of New Indium Bismuth Sulfide Halides $InBi_2S_4Cl$ and $InBi_2S_4Br$. *Mater. Res. Bull.* **1976**, *11*, 183-187.
33. Ohmasa, M.; Mariolac.K. Crystal-Structure of $(Pb_{1-X}, Bi_x)Bi_2Cu_2Cu_{2-X}S_5I_2$(X=0.88). *Acta Crystallogr. B* **1974**, *30*, 2640-2643.
34. Ibanez, A.; Jumas, J. C.; Olivierfourcade, J.; Philippot, E. Synthesis and Classification of Tin and Antimony Chalcogenoidides. *Rev. Chim. Miner.* **1984**, *21*, 344-357.
35. Beck, J.; Hedderich, S.; Kollisch, K. Hg_3AsE_4X (E = S, Se; X = Cl, Br, I), a family of isotypic compounds with an acentric, layered structure. *Inorg. Chem.* **2000**, *39*, 5847-50.
36. Olivierfourcade, J.; Jumas, J. C.; Maurin, M.; Philippot, E. A New Sulfoiodide of Tin and Antimony - Structure Investigation. *Z. Anorg. Allg. Chem.* **1980**, *468*, 91-98.
37. Doussier, C.; Moelo, Y.; Leone, P.; Meerschaut, A.; Evain, M. Crystal structure of $Pb_2SbS_2I_3$, and re-examination of the crystal chemistry within the group of (Pb/Sn/Sb-) chalcogeno-iodides. *Solid State Sci.* **2007**, *9*, 792-803.
38. Starosta, V. I.; Kroutil, J.; Benes, L. Preparation and Fundamental Physical-Properties of $Sn_2SbS_2I_3$ and $Pb_2SbS_2I_3$ Compounds. *Cryst. Res. Technol.* **1990**, *25*, 1439-1442.

39. Liang, I. C.; Bilc, D. I.; Manoli, M.; Chang, W. Y.; Lin, W. F.; Kyratsi, T.; Hsu, K. F. Syntheses, crystal Structures and electronic Structures of new metal chalcoiodides Bi_2CuSe_3I and $Bi_6Cu_3S_{10}I$. *J. Solid State Chem.* **2016**, *234*, 1-8.
40. Zelenski, M.; Balic-Zunic, T.; Bindi, L.; Garavelli, A.; Makovicky, E.; Pinto, D.; Vurro, F. First occurrence of iodine in natural sulfosalts: The case of mutnovskite, Pb_2AsS_3(I,Cl,Br), a new mineral from the Mutnovsky volcano, Kamchatka Peninsula, Russian Federation. *American Mineralogist* **2006**, *91*, 21-28.
41. Haasewes.W. Crystalline-Structure of Bismuth Sulfide Iodide (BiSI). *Naturwissenschaften* **1973**, *60*, 474-474.
42. Inorganic Crystal Structure Database. In *Inorganic Crystal Structure Database*, 2016 ed.; FIZ Karlsruhe/NIST: FIZ Karlsruhe 2016; Vol. Version 3.4.0.
43. Altermatt, I. D. B. D. Bond-valence parameters obtained from a systematic analysis of the Inorganic Crystal Structure Database. *Acta. Cryst.* **1985**, *B41*, 244-247.
44. Wood, C.; Chmielewski, A.; Zoltan, D. MEASUREMENT OF SEEBECK COEFFICIENT USING A LARGE THERMAL-GRADIENT. *Rev. Sci. Instrum.* **1988**, *59*, 951-954.
45. Blöchl, P. E. Projector augmented-wave method. *Phys. Rev. B* **1994**, *50*, 17953.
46. Kresse, G.; Furthmuller, J. Efficient iterative schemes for ab initio total-energy calculations using a plane-wave basis set. *Phys. Rev. B Condens Matter.* **1996**, *54*, 11169-11186.
47. Kresse, G.; Hafner, J. Ab initio molecular-dynamics simulation of the liquid-metal-amorphous-semiconductor transition in germanium. *Phys. Rev. B Condens Matter.* **1994**, *49*, 14251-14269.
48. Perdew, J. P.; Burke, K.; Ernzerhof, M. Generalized gradient approximation made simple. *Phy.Rev. Lett.* **1996**, *77*, 3865-3868.
49. Dolgikh, V. A. *Izv. Akad. Nauk SSSR, Neorg. Mater.,* **1985**, *21*, 1211–1214.
50. Krebs, B. Crystal-Structures of Pb_4SeBr_6, $Pb_5S_2I_6$, and $Pb_7S_2Br_{10}$. *Z. Anorg. Allg. Chem.* **1973**, *396*, 137-151.
51. Kanatzidis, M. G. Structural evolution and phase homologies for "design" and prediction of solid-state compounds. *Acc. Chem. Res.* **2005**, *38*, 359-68.
52. Mrotzek, A.; Kanatzidis, M. G. "Design" in solid-state chemistry based on phase homologies. The concept of structural evolution and the new megaseries $A_m[M_{1+l}Se_{2+l}]_{2m}[M_{2l+n}Se_{2+3l+n}]$. *Acc. Chem. Res.* **2003**, *36*, 111-9.
53. Moulder, J. F.; Stickle, W. F.; Sobol, P. E.; Bomben, K., *Handbook of X-ray photoelectron spectroscopy.*

. Perkin-Elmer Corporation: Minnesota. , 1995; Vol. 2nd.
54. Alonzo, G.; Bertazzi, N.; Ferraro, J. R.; Furlani, A.; Iucci, G.; Polzonetti, G.; Russo, M. V. Mossbauer, Far-Infrared, and XPS Investigations of $SnCl_2$ and $SnCl_4$ Introduced in Polyconjugated Monosubstituted Acetylene Matrices. *App. Spectros.* **1995**, *49*, 237-240.
55. Umari, P.; Mosconi, E.; De Angelis, F. Relativistic GW calculations on $CH_3NH_3PbI_3$ and $CH_3NH_3SnI_3$ perovskites for solar cell applications. *Sci. Rep.* **2014**, *4*, 4467.
56. Pyykko, P. Relativistic Effects in Structural Chemistry. *Chem. Rev.* **1988**, *88*, 563-594.
57. Perdew, J. P.; Chevary, J. A.; Vosko, S. H.; Jackson, K. A.; Perderson, M. R.; Singh, D. J.; Fiolhais, C. Atoms, molecules, solids, and surfaces: Applications of the generalized gradient approximation for exchange and correlation. *Phys. Rev. B* **1992**, *46*, 6671-6687.

58. Perdew, J. P.; Levy, M. Physical Content of the Exact Kohn-Sham Orbital Energies - Band-Gaps and Derivative Discontinuities. *Phys. Rev. Lett.* **1983**, *51*, 1884-1887.
59. Islam, S. M.; Vanishri, S.; Li, H.; Stoumpos, C. C.; Peters, J. A.; Sebastian, M.; Liu, Z. F.; Wang, S.; Haynes, A. S.; Im, J.; Freeman, A. J.; Wessels, B.; Kanatzidis, M. G. $Cs_2Hg_3S_4$: A Low-Dimensional Direct Bandgap Semiconductor. *Chem. Mater.* **2015**, *27*, 370-378.

60. Islam, S. M.; Im, J.; Freeman, A. J.; Kanatzidis, M. G. Ba_2HgS_5-A Molecular Trisulfide Salt with Dumbbell-like $(HgS_2)^{2-}$ Ions. *Inorg. Chem.* **2014**, *53*, 4698-4704.

TOC: